Journal of Statistical Physics, Vol. 78, Nos. 3/4, 1995

Deposition–Evaporation Stochastic Systems in Two and Higher Dimensions

Niu-Niu Chen,[1,2] M. D. Grynberg,[1,3] and R. B. Stinchcombe[1]

Received April 29, 1994; final August 17, 1994

We study the stochastic dynamics of deposition–evaporation cooperative processes of dimers, trimers, etc., in two- and higher-dimensional lattices. The dimer system in bipartite lattices allows for an exact solution of dynamic correlations and scaling functions by means of a quantum spin equivalence. Autocorrelations exhibit a diffusive asymptotic kinetics and crossovers of different dynamic regimes in highly anisotropic lattices. Monte Carlo simulations combined with finite-size scaling arguments support the validity of the diffusive picture in more general situations. Steady-state coverages and diffusion constants are obtained using mean-field approaches, spin wave calculations, and random walk analyses in nearly jammed configurations.

KEY WORDS: Deposition; evaporation; jamming; two-dimensional; dimer.

1. INTRODUCTION

There is much current interest in problems of stochastic dynamics,[1] ranging from idealized probabilistic cellular automata[2] and nonlinear dynamic field equations[3] to driven[4] and self-organized systems.[5,6]

An important class of stochastic dynamical systems which share many characteristics emphasized in such studies is the set of deposition–evaporation systems.[7,8] A subset consists of the dimer deposition models, well known since the work of Flory and Renyi for their jamming behavior, which is an indication of extremely strong fluctuation effects.[8-10] These deposition–evaporation systems are useful models for such processes as

[1] Theoretical Physics, Department of Physics, University of Oxford, Oxford OX1 3NP, U.K.
[2] Present address: Physics Department, Rutgers University, Piscataway, New Jersey 08855. E-mail: nnchen@physics.rutgers.edu.
[3] Present address: Departamento de Fisica, Comision Nacional de Energia Atomica, (1429) Buenos Aires, Argentina. E-mail: mgrynber@cnea.edu.ar.

822/78/3-4-20

catalysis, etc., which have very important real applications.[11–15] In such contexts the coverage on the jammed states (i.e., the nature of the so-called "poisoning") is important to study, and so is the rate of approach to these states.

Recent studies on one-dimensional models have shown that systems with evaporation (after possibly recombination) as well as deposition are much richer compared to deposition-only models, particularly when the general k-mer case is considered ($k = 1, 2, 3,...$ correspond respectively to monomers, dimers, trimers, etc.).[16] The models still retain jamming and other strong fluctuation effects, but can also have a slow universal dynamics of diffusive type and also show strong nonergodicity for $k \geqslant 3$, related to the existence of exponentially many jammed states and disconnected subspaces.[17]

In the models with deposition alone, the approach is typically exponential in time.[18] But in the study of the one-dimensional deposition–evaporation models it was found by Monte Carlo simulations that large classes have universal power law decay to the steady states.[16] This was explained analytically by an exact solution for a special case, and in terms of Goldstone symmetry present in general in the systems.[19],[4] This symmetry is related to the existence of quantities conserved under the deposition–evaporation process. But it is also apparent as a type of continuous rotation symmetry in pseudospin Hamiltonians which express the dynamics in terms of the flip of fictitious spins representing occupancy or vacancy of a site by spin up or spin down there. The resulting Hamiltonians are of quantum spin-1/2 type and generalize in a highly nontrivial way the isotropic Heisenberg Hamiltonian, which, after a sublattice mapping, represents the special case for dimers deposited and evaporated with equal rates. The Goldstone symmetry is present in the one-dimensional case whether or not deposition and evaporation rates ($\varepsilon, \varepsilon'$) are equal, but it does require depositing and evaporating k-mers with the same k. As discussed more generally in Section 2.2, the related conserved quantities are the differences of sublattice occupations. The corresponding density differences must then satisfy continuity equations containing the divergence of associated currents. These currents have to vanish in the limit where densities are uniform on each sublattices. This suggests that related rates should vanish in the limit of long wavelengths. This is the well-known route from conservation laws to slow dynamics,[19] familiar in such cases as diffusion.

It is clearly of crucial importance to extend the study of the deposition-evaporation process from one to two and higher dimensions for the

[4] For fuller accounts see, e.g., refs. 20.

problems of catalysis on real surfaces, etc. That is the object of the present paper. It will be shown that many characteristics of the one-dimensional behavior carry over to the higher-dimensional case. These include the existence of many jammed and steady states and the (related) occurrence of strongly nonergodic behavior.

But whereas in one dimension all systems with deposition and evaporation of k-mers with the same k have the slow power law approach to the steady states,[16] in two dimensions whether or not this occurs depends on lattice type and k-mer shape. For example, for dimers ($k=2$), all bipartite lattices have the slow dynamics. The splitting of dynamic behavior according to lattice and k-mer type is evident in Monte Carlo simulation. It can be explained in terms of the effective quantum spin Hamiltonians which apply in the two-dimensional systems by extending the Goldstone broken symmetry argument.

Another way in which the two-dimensional case differs qualitatively from the one-dimensional one is in effects arising from lattice anisotropy. If a uniaxially anisotropic k-mer (e.g., a dimer or linear trimer) is deposited and evaporated with rates which depend on the orientation of the axes with respect to crystal axes, both the steady states and the time-dependent approach to them will be modified. A qualitative change here is the occurrence of crossovers in the decay, for large anisotropies, or in the finite-size scaling behavior for different limiting scales in the two lattice directions. Apart from such differences, the finite-size scaling studies show universal time decay of the same sort as seen in the one-dimensional case.

In this respect the dimer system with equal evaporation and deposition rates shows a behavior typical of all members of the common universality class. However, as in the one-dimensional case, this system is amenable to an exact calculation of time-dependent correlation functions. This is because the correlation function only involves the steady states and certain particular excited states, which are rotated versions of the parallel-spin ground states and the rotated *single*-spin-wave states, respectively, of the equivalent isotropic Heisenberg model. The associated generalized spin wave excitations are the Goldstone bosons of this system. The exact correlation function calculated with this approach provides a detailed description of the anisotropy, crossover, etc., for the dimer system with equal rates, and furthermore it gives the finite-size scaling function in the long-time regime when only the low-lying excited states are involved. The scaling function agrees very well with numerical finite-size scaling results for dimers with equal rates and also for the nonequal rate case. More remarkably, the scaling function appears also to describe the asymptotic finite-size scaling behavior of k-mer systems with $k>2$ provided they

have the Goldstone symmetry. An example is triangular trimers on the triangular lattice.

When the behavior of the two-dimensional case does not differ qualitatively from the one-dimensional one (e.g., when it shares an isotropic diffusive long-time decay) quantitative differences in detailed behavior may remain, and are of some interest. So the correlation function, diffusion constant, etc., have been investigated by numerical studies, and in some cases evaluated by a variety of analytic approaches.

The specific analytic techniques employed include some, like generalized spin wave approaches and broken symmetry arguments, based on the quantum spin description. Techniques using the particle description include a mean-field approach which provides particle currents in terms of local densities and hence, via the continuity equation, a nonlinear equation for the densities. This is good when fluctuation effects are not severe, e.g., for dimers on bipartite lattices away from the Flory limit ($\varepsilon' = 0$). The diffusive description which results from linearizing near steady states works well for the dimer system in the long-time limit (whether or not $\varepsilon = \varepsilon'$, but provided neither rate is zero). In another particle-picture approach, for k-mers with arbitrary k, the dynamics of small active patches on an otherwise jammed simple background can be exactly described by generalized random walks. This approach gives further evidence for diffusion behavior and provides diffusion constants. It shows that the mean-field diffusive description of dimers is exact in cases where the two methods have been compared. The numerical studies are based on Monte Carlo approaches, combined with finite-size scaling to allow the slow dynamics to be investigated without running prohibitively large computations.

The layout of the remainder of this paper is as follows. Section 2 describes the two-dimensional deposition–evaporation systems considered in this study and gives the master equation governing their stochastic time evolution. The pseudospin formalism is here developed and the quantum spin Hamiltonian is provided for the general class of system, i.e., k-mers with arbitrary shape, deposited and evaporated with anisotropic rates ε, ε' on arbitrary regular two-dimensional lattices. Conserved quantities and continuous symmetries of the Hamiltonian are also discussed in this section. Section 3 provides the exact analytic treatment of the dynamic correlation functions of the dimer model for equal, but possibly anisotropic rates, for infinite and bipartite lattices. A consequence is the exact finite-size scaling function for the long-time regime. The results are compared in Section 4 with Monte Carlo simulations combined with finite-size scaling analysis for dimers with equal rates. The numerical investigations of the other (larger k, $\varepsilon \neq \varepsilon'$) generalizations within the universality class are also reported in Section 4 and compared with the scaling function derived in

Section 3. Section 4 includes also simulation results for an example, dimers on the triangular lattice, which does not have the Goldstone symmetry. This shows fast (exponential) time decay, as expected from the general arguments given earlier. The section concludes with steady-state coverage data for various cases.

Section 5 gives a variety of theoretical approaches which are very effective for certain situations. The first of these, given in Section 5.1, is the mean-field description. It leads to diffusive decay at long times and provides values for diffusion constants. These can be seen to be exact for dimers on bipartite lattices by comparing with exact treatments for special backgrounds provided in Sections 5.2 and 5.3. Section 5.2 gives the exact spin wave treatment for dimers on the square lattice (with rates which can be unequal and/or anisotropic). Section 5.3 contains the random walk approaches for nearly jammed configurations, providing exact diffusion behavior and exact results for diffusion constants for dimers on any bipartite lattice. Again the rates $\varepsilon, \varepsilon'$ can be unequal or anisotropic. The results are illustrated with details for square and honeycomb lattices. Section 5.3 also gives the random walk description of triangular trimers on the triangular lattice and discusses in less detail some other cases involving plaquette k-mers. Section 6 is a concluding discussion gathering together the main results of the paper and commenting on extensions desirable for a comprehensive understanding of such systems, particularly in the context of catalysis and of stochastic and driven systems in general.

2. THE MASTER EQUATION AND RELATED SYMMETRIES OF THE TRANSITION OPERATOR

The stochastic dynamical processes under consideration here are random deposition–evaporation of k-mers (where $k = 1, 2, 3,$ etc.) on various d-dimensional lattices. At a given time, deposition with rate ε of k-mers of particular shape is successful only if the randomly-chosen k sites of the corresponding shape on the lattice are vacant. Similarly, the evaporation processes occur with rate ε', provided that all the k selected lattice sites are unoccupied. This process will then repeat in successive later times with different sites being chosen at random. Since any k occupied sites forming the given shape on the lattice can be evaporated together, this gives rise to the reconstruction of the k-mer groups and redistribution of particles, and hence an effective particle hopping or diffusion. In this paper, we mainly consider dimers of two adjacent sites on 2D square, honeycomb, or 3D cubic lattices, and trimers in the shape of triangular plaquettes on the 2D triangular lattice.

2.1. The Transition Operator

The time dependence of these stochastic processes can be described by the master equation, which governs the time evolution of the probabilities $P(s, t)$ of finding the system in a certain configuration $|s\rangle$ at time t. If $W(s \to s')$ denotes the rate or transition probability per unit time at which configuration $|s\rangle$ evolves to $|s'\rangle$, the master equation is

$$\frac{\partial}{\partial t} P(s, t) = \sum_{s'} [W(s' \to s) P(s', t) - W(s \to s') P(s, t)] \tag{1}$$

Since the basis vectors $|s\rangle$ form an orthonormal set, the ensemble-averaged state vector of the system at time t can be defined by

$$|P(t)\rangle = \sum_{s} P(s, t) |s\rangle \tag{2}$$

It is then easy to check that the master equation (1) can now be written for the state vector $|P(t)\rangle$ as

$$\frac{\partial}{\partial t} |P(t)\rangle = -H |P(t)\rangle \tag{3}$$

where the transition operator H (or "Hamiltonian") is defined in terms of its matrix elements:

$$\langle s'| H |s\rangle = -W(s \to s'), \qquad s' \neq s \tag{4}$$

$$\langle s| H |s\rangle = \sum_{s' \neq s} W(s \to s') \tag{5}$$

A formal integration of the above equation yields the solution for the state vector

$$|P(t)\rangle = \exp[-H(t - t_0)] |P(t_0)\rangle \tag{6}$$

The steady states of our dynamical system correspond to the ground states of H in each disconnected subspace, all with the zero eigenvalue $E_0 = 0$. Any eigenvalues with positive real parts $E > 0$ correspond to decaying states with lifetime $1/E$. It is also worthwhile to note that every column of matrix H adds up to zero, $\sum_{s'} \langle s'| H |s\rangle = 0$, due to probability conservation.

We now explore the analogy between our deposition–evaporation model and the quantum spin-1/2 system. Using the eigenvalues of the Pauli

matrices $\sigma_{\mathbf{r}}^z$ 1 or -1 to denote site $\mathbf{r}$ occupied or vacant, we can describe the particle configuration of the lattice with total number of sites N by

$$|s\rangle = |\sigma_{\mathbf{r}_1}^z, \sigma_{\mathbf{r}_2}^z, \sigma_{\mathbf{r}_3}^z, \ldots, \sigma_{\mathbf{r}_N}^z\rangle$$

A single deposition or evaporation process then corresponds to the action of

$$\sigma_{\mathbf{r}}^+ \prod_{j=1}^{k-1} \sigma_{\mathbf{r}+\boldsymbol{\delta}_j}^+$$

or its Hermitian conjugate, where the site $\mathbf{r}$ and the sites corresponding to the $k-1$ vectors $\boldsymbol{\delta}_j$ form the designated shape of k-mers under consideration on the lattice. The off-diagonal part of H, which connects two different states $|s\rangle$ and $|s'\rangle$ through a single deposition–evaporation process [see Eq. (4)], should therefore take the form

$$\sum_{s,s'}{}' |s'\rangle\langle s'| H |s\rangle\langle s| = -\sum_{\mathbf{r},\{\boldsymbol{\delta}_j\}} \left(\varepsilon \sigma_{\mathbf{r}}^+ \prod_{j=1}^{k-1} \sigma_{\mathbf{r}+\boldsymbol{\delta}_j}^+ + \varepsilon' \sigma_{\mathbf{r}}^- \prod_{j=1}^{k-1} \sigma_{\mathbf{r}+\boldsymbol{\delta}_j}^- \right) \quad (7)$$

where the prime on the sum on the left-hand side denotes the exclusion of $s = s'$ terms, whereas the set $\{\boldsymbol{\delta}_j\}$ indicates all the possible vectors joining the site $\mathbf{r}$ with each of the $k-1$ remaining sites of a k-mer cluster with an arbitrarily chosen orientation.

From Eq. (5) the diagonal part of H counts the total number of ways in which configuration $|s\rangle$ can evolve to different states $|s'\rangle$ through a single deposition–evaporation process. This number is the total number of k-down-spin (vacant site) groups in state $|s\rangle$ which form the designated shape of k-mers under consideration, and is counted by the operator

$$\sum_{\mathbf{r},\{\boldsymbol{\delta}_j\}} (1 - \sigma_{\mathbf{r}}^+ \sigma_{\mathbf{r}}^-) \prod_{j=1}^{k-1} (1 - \sigma_{\mathbf{r}+\boldsymbol{\delta}_j}^+ \sigma_{\mathbf{r}+\boldsymbol{\delta}_j}^-)$$

Similarly, the operator

$$\sum_{\mathbf{r},\{\boldsymbol{\delta}_j\}} \sigma_{\mathbf{r}}^+ \sigma_{\mathbf{r}}^- \prod_{j=1}^{k-1} \sigma_{\mathbf{r}+\boldsymbol{\delta}_j}^+ \sigma_{\mathbf{r}+\boldsymbol{\delta}_j}^-$$

counts the total number of realizable evaporation attempts, or of the k-up-spin groups. We can therefore write the diagonal part of H as

$$\sum_s |s\rangle\langle s| H |s\rangle\langle s| = \sum_{\mathbf{r},\{\boldsymbol{\delta}_j\}} \varepsilon (1 - \sigma_{\mathbf{r}}^+ \sigma_{\mathbf{r}}^-) \prod_{j=1}^{k-1} (1 - \sigma_{\mathbf{r}+\boldsymbol{\delta}_j}^+ \sigma_{\mathbf{r}+\boldsymbol{\delta}_j}^-) + \sum_{\mathbf{r},\{\boldsymbol{\delta}_j\}} \varepsilon' \sigma_{\mathbf{r}}^+ \sigma_{\mathbf{r}}^- \prod_{j=1}^{k-1} \sigma_{\mathbf{r}+\boldsymbol{\delta}_j}^+ \sigma_{\mathbf{r}+\boldsymbol{\delta}_j}^- \quad (8)$$

It can be easily shown that the total transition operator H, (7)+(8), reduces to the form of ferromagnetic Heisenberg Hamiltonian with nearest-neighbor interactions when we consider dimers ($k=2$) on bipartite lattices with *equal* deposition and evaporation rates ($\varepsilon=\varepsilon'$). This special case will be studied in more detail in Section 3.

2.2. Conserved Quantities and Related Symmetries

In the Ising or particle representation, a set of $k-1$ independent constants of motion can be readily obtained. Assuming the lattice is *k-partite*, the system can be divided into k sublattices Λ_α, $\alpha=1, 2,..., k$, such that each deposition or evaporation process involves k sites belonging to each of the different Λ_α sublattices, so that wherever placed on the lattice the k-mer covers one site of each sublattice. For any state $|s\rangle$ define $M_\alpha \equiv \sum_{\mathbf{r}\in\alpha} \sigma_{\mathbf{r}}^z |s\rangle$ as the total "magnetization" of sublattice Λ_α. Therefore the dynamics clearly leaves invariant $k-1$ independent differences $M_\alpha - M_k$.

This family of conservation laws can be also obtained by noting that the most general constant of motion involving only z components (excluding a trivial additive constant) is of the form

$$Q=\sum_{\mathbf{r}} C_{\mathbf{r}}\sigma_{\mathbf{r}}^z \tag{9}$$

By considering $[H, Q]=0$ it is straightforward to show that

$$C_{\mathbf{r}}+\sum_{j=1}^{k-1} C_{\mathbf{r}+\boldsymbol{\delta}_j}\equiv 0 \quad \forall \mathbf{r} \tag{10}$$

where $\boldsymbol{\delta}_j$ are the vectors joining the site $\mathbf{r}$ with each of the $k-1$ remaining sites of a k-mer cluster with a given arbitrary orientation. This set of linear equations results in $k-1$ independent conserved quantities formed by linear combinations of $Q_1, Q_2,..., Q_{k-1}$, where

$$Q_j=\sum_{\mathbf{r}} \lambda_j^{n(\mathbf{r})}\sigma_{\mathbf{r}}^z, \qquad \lambda_j \equiv \exp(i2\pi j/k) \tag{11}$$

($1\leqslant j<k$) and $n(\mathbf{r})=\alpha$ if $\mathbf{r}$ belongs to the Λ_α sublattice, $\alpha=1, 2,..., k$. Equivalently, each Q can be written in terms of appropriate linear combinations of $M_\alpha - M_k$ ($\alpha=1, 2,..., k-1$), which in turn can take the values $(-2N/k, -2N/k+2,..., 2N/k-2, 2N/k)$. In particular, for the case $k=2$ the resulting single conserved quantity is a staggered magnetization which can take $N+1$ values. As will be discussed in Section 3, this is related to the total magnetization of the isotropic Heisenberg ferromagnet.

The above constants of motion are the only ones involving *local* combinations of spin operators. However, it is important to point out that for $k \geqslant 3$ other studies in one-dimensional systems reveal the existence of large quantities of *nonlocal* conservation laws whose number grows exponentially with the size of the system.[16,17] The dynamics is then partitioned into an equally large number of invariant subspaces and in some cases may exhibit different asymptotic behaviors. Indeed, this is a quite uncommon feature in systems without quenched disorder.

From a more fundamental point of view the conservation of $M_\alpha - M_k$ arises from a continuous symmetry of the time evolution generator for general values of k, ε, and ε'. Additionally, this provides an understanding of the slow asymptotic dynamics seen in general. We first note that under a rotation by an angle $\varphi_{\mathbf{r}}$ around the z axis the $\sigma_{\mathbf{r}}^x$ and $\sigma_{\mathbf{r}}^y$ Pauli matrices transform according to

$$\sigma_{\mathbf{r}}^x \to \sigma_{\mathbf{r}}^x \cos\varphi_{\mathbf{r}} - \sigma_{\mathbf{r}}^y \sin\varphi_{\mathbf{r}}, \qquad \sigma_{\mathbf{r}}^y \to \sigma_{\mathbf{r}}^x \sin\varphi_{\mathbf{r}} + \sigma_{\mathbf{r}}^y \cos\varphi_{\mathbf{r}}$$
$$\Rightarrow \sigma_{\mathbf{r}}^{\pm} \to \exp(\pm i\varphi_{\mathbf{r}})\, \sigma_{\mathbf{r}}^{\pm} \tag{12}$$

This rotation leaves the off-diagonal part of the transition operator H unaltered provided that

$$\varphi_{\mathbf{r}} + \sum_{j=1}^{k-1} \varphi_{\mathbf{r}+\delta_j} \equiv 0 \quad \forall \mathbf{r} \tag{13}$$

where the vectors $\boldsymbol{\delta}_j$ are taken as in Eq. (10). This condition can be fulfilled for k-partite lattices using common rotation angles $\varphi_{\mathbf{r}} = \varphi_\alpha$ for all spins $\mathbf{r}$ on sublattice Λ_α subject to the constraint

$$\sum_{\alpha=1}^{k} \varphi_\alpha = 0 \tag{14}$$

Therefore the evolution operator H remains invariant under this *continuous* z symmetry with $k-1$ degrees of freedom, as the diagonal terms of H are also not affected by such rotation. The infinitesimal generator of this symmetry is given by

$$S \equiv \sum_{\alpha=1}^{k} \varphi_\alpha M_\alpha^z, \qquad M_\alpha^z \equiv \sum_{\mathbf{r}\in\Lambda_\alpha} \sigma_{\mathbf{r}}^z \tag{15}$$

Since $H = \exp(iS/2)\, H \exp(-iS/2)$, it follows that $[H, S] = 0$ and therefore S is a conserved quantity. From Eqs. (14) and (15) it is clear that S can be written in terms of $k-1$ independent angles, namely

$$S = \sum_{\alpha=1}^{k-1} \varphi_\alpha (M_\alpha^z - M_k^z) \tag{16}$$

As consequence of this continuous symmetry we thus recover the $k-1$ independent conserved quantities $M_\alpha - M_k$ already identified by applying $M_\alpha^z - M_k^z$ to an arbitrary initial state $|s\rangle$.

It is well known that continuous symmetries, conserved quantities, and slow kinetics are closely interrelated. According to the Goldstone theorem, whenever a ground or steady state of H breaks the continuous symmetry discussed above, the existence of a gapless band of Goldstone modes can be inferred. These Goldstone excitations are in turn reflected in the slow asymptotic dynamics observed in our deposition–evaporation models.

We now show how a class of steady states which break the Goldstone symmetry can be constructed. Let us introduce the operators $\xi_{\mathbf{r}} \equiv \gamma\sigma_{\mathbf{r}}^+ + \gamma^{-1}\sigma_{\mathbf{r}}^-$, $\gamma = (\varepsilon/\varepsilon')^{1/k}$ arising from pseudorotations of the original spins. The eigenvalues of these operators are $m_{\mathbf{r}} = \pm 1$ and their normalized eigenstates $|\xi_{\mathbf{r}}\rangle$ are given by

$$|\xi_{\mathbf{r}}\rangle = \frac{\gamma}{(\gamma^2+1)^{1/2}}\left(1 + \frac{m_{\mathbf{r}}}{\gamma}\sigma_{\mathbf{r}}^-\right)|\uparrow\rangle_{\mathbf{r}} \tag{17}$$

It can be checked easily that

$$H = \sum_{\mathbf{r},\{\delta_j\}} \left\{ \left[\frac{\varepsilon}{2^k}(1-\sigma_{\mathbf{r}}^z)\prod_{j=1}^{k-1}(1-\sigma_{\mathbf{r}+\delta_j}^z) + \frac{\varepsilon'}{2^k}(1+\sigma_{\mathbf{r}}^z)\prod_{j=1}^{k-1}(1+\sigma_{\mathbf{r}+\delta_j}^z) \right] \times (1-\xi_{\mathbf{r}})\prod_{j=1}^{k-1}(1-\xi_{\mathbf{r}+\delta_j}) \right\} \tag{18}$$

where the set of vectors $\{\boldsymbol{\delta}_j\}$ are taken as in Eq. (7). If $|0\rangle$ denotes the state with all spins up, steady states $|\xi\rangle$ of H (with vanishing eigenvalue) can be obtained as

$$|\xi\rangle = \frac{\gamma^N}{(\gamma^2+1)^{N/2}}\prod_{\mathbf{r}}\left(1 + \frac{m_{\mathbf{r}}}{\gamma}\sigma_{\mathbf{r}}^-\right)|0\rangle \tag{19}$$

provided that $\prod_{\mathbf{r}} m_{\mathbf{r}} = 1$. Applying the z-rotation generator S of Eq. (15) to these states $|\xi\rangle$ generates *new* (unnormalized) steady states of the form

$$\exp\left(\frac{iS}{2}\right)|\xi\rangle = \prod_{\mathbf{r}}\left[\exp\left(\frac{i\varphi_{\mathbf{r}}}{2}\right) + \frac{m_{\mathbf{r}}}{\gamma}\exp\left(\frac{-i\varphi_{\mathbf{r}}}{2}\right)\sigma_{\mathbf{r}}^-\right]|0\rangle \tag{20}$$

where $\varphi_{\mathbf{r}} = \varphi_\alpha$, $\mathbf{r} \in \Lambda_\alpha$ are taken as in Eq. (14), and $m_{\mathbf{r}}$ as in Eq. (19). Note that by exploiting the $k-1$ continuous degrees of freedom of the set $\{\varphi_\alpha\}$, even more general steady states can be produced.

In what follows we will discuss the consequences of the Goldstone symmetry breaking, which will be reflected in the diffusive decay observed in our deposition–evaporation models.

3. DYNAMIC CORRELATION FUNCTIONS OF THE DIMER MODEL ($\epsilon = \epsilon'$)

In this section we calculate analytically dynamic correlation functions for the special cases of dimers on *bipartite* lattices with equal deposition and evaporation rates. This equal-rate condition enables us to map the system into the spin-1/2 Heisenberg model with nearest-neighbor coupling (for dimers). The bipartite lattice structure then permits fully jammed nonfrustrated Néel states from which other nonjammed steady states can be generated. These features allow for an exact solution even in spatially anisotropic cases. The more general k-mer problem in a variety of different situations will be considered in the following sections using alternative approaches.

In the case of dimers with adsorption–desorption in a d-dimensional bipartite lattice $\Lambda = \Lambda_a + \Lambda_b$, it is convenient to introduce the following sublattice mapping:

$$\begin{aligned} &\tau_{\mathbf{r}} \equiv \sigma_{\mathbf{r}}, \qquad \mathbf{r} \in \Lambda_a \\ &\tau_{\mathbf{r}} \equiv (\sigma_{\mathbf{r}}^x, -\sigma_{\mathbf{r}}^y, -\sigma_{\mathbf{r}}^z), \qquad \tau_{\mathbf{r}}^{\pm} \equiv \sigma_{\mathbf{r}}^{\mp}, \qquad \mathbf{r} \in \Lambda_b \end{aligned} \tag{21}$$

Therefore, for $\varepsilon = \varepsilon'$ it can be easily checked that the time evolution generator referred to in Section 2.1 [Eqs. (7) and (8)] can be cast in terms of a spin-1/2 isotropic Heisenberg ferromagnet,

$$\mathscr{H} = -\tfrac{1}{2} \sum_{\mathbf{r},j} \varepsilon_{\delta_j} (\tau_{\mathbf{r}} \cdot \tau_{\mathbf{r}+\delta_j} - 1) \tag{22}$$

where j runs over all nearest-neighbor sites $\mathbf{r} + \boldsymbol{\delta}_j$ of $\mathbf{r}$. In particular, the two fully jammed Néel states of the original system correspond to the two ferromagnetic configurations in the τ-particle or sublattice representation (21).

Due to the isotropic nature of the interactions, the dynamics of the deposition–evaporation process leaves invariant all the components of the total angular momentum $\mathbf{T} = \frac{1}{2} \sum_{\mathbf{r}} \tau_{\mathbf{r}}$, i.e., $[\mathscr{H}, \mathbf{T}] = 0$. As a consequence of this full rotational symmetry, the calculation of time-dependent correlations and dynamic scaling functions is simplified remarkably, thus enabling an exact solution in the steady state. It is well known that the isotropic Heisenberg ferromagnet $\mathscr{H}$ has a low-lying band of gapless or Goldstone

modes. As will be shown below, these excitations are ultimately responsible for the slow asymptotic dynamic behavior reflected in long-time tail correlation functions.

The conservation of $\mathbf{T}$ is a special feature arising only in the dimer model with *equal* deposition–evaporation rates. Although for $\varepsilon \neq \varepsilon'$, T^z is still conserved, T^x and T^y do not commute with $\mathscr{H}$ and therefore the approach we are going to discuss can no longer be applied. However, as was indicated in Section 2, collective continuous symmetries around the z axis are still present and a diffusive kinetics might be expected as well. In fact, numerical simulations combined with finite-size scaling arguments to be introduced in Section 4 provide evidence of universality on ε and ε'. For the sake of simplicity we will consider the case of a hypercubic lattice, although the same arguments apply for arbitrary bipartite geometries where the sublattice mapping (21) is well defined. Moreover, quenched disordered systems can be equally analyzed as long as the full rotational invariance is not violated.

3.1. The Steady State

For a given number of τ-particles with specified total magnetization $T^z = N/2 - m$ in the sublattice mapped system, the corresponding steady state $|\psi_m\rangle$ can be obtained by applying m times the lowering operator $T^- = T^x - iT^y$ to the fully jammed ferromagnetic configuration $|\psi_0\rangle$ with all N spins up (i.e., Néel state of the original system). Recalling that the angular momentum algebra imposes

$$T^- \,|T, T^z\rangle = [(T+T^z)(T-T^z+1)]^{1/2}\,|T, T^z-1\rangle$$

we find a normalized steady state in the m-down-spin sector as

$$|\psi_m\rangle = B_m (T^-)^m\,|\psi_0\rangle = m!\, B_m \sum_{j_1<j_2<\cdots<j_m} \sum \cdots \sum \tau^-_{\mathbf{r}_{j_1}} \tau^-_{\mathbf{r}_{j_2}} \cdots \tau^-_{\mathbf{r}_{j_m}}\,|\psi_0\rangle \tag{23}$$

where the normalization factor B_m is given by

$$B_m = \left[\frac{(N-m)!}{m!\,N!}\right]^{1/2} \tag{24}$$

Since $[\mathscr{H}, T^-] = 0$, clearly $|\psi_m\rangle$ is a steady state and is an equally weighted linear combination of configurations with m τ-particles. Note that for a given sublattice magnetization (specified by the initial conditions) there is a unique steady state implying that T^z is in turn the unique constant of motion of the *original* system in the particle representation. Thus, there are $N+1$ dynamically invariant subspaces. This holds also for $\varepsilon \neq \varepsilon'$

as the number of total invariant subspaces and the particular configurations contained in them are independent of ε and ε' provided that both rates have nonzero values.

For $\varepsilon = \varepsilon'$ the steady coverage θ_0 is calculated as

$$\theta_0 = \frac{1}{N} \sum_{\mathbf{r} \in \Lambda_a} \langle \psi_m | \hat{n}_\mathbf{r} | \psi_m \rangle + \frac{1}{N} \sum_{\mathbf{r} \in \Lambda_b} \langle \psi_m | (1 - \hat{n}_\mathbf{r}) | \psi_m \rangle \tag{25}$$

where $\hat{n}_\mathbf{r} = \tau_\mathbf{r}^+ \tau_\mathbf{r}^-$. Since

$$\langle \psi_m | \hat{n}_\mathbf{r} | \psi_m \rangle \equiv \binom{N-1}{m} \Big/ \binom{N}{m}$$

and

$$\langle \psi_m | (1 - \hat{n}_\mathbf{r}) | \psi_m \rangle \equiv \binom{N-1}{m-1} \Big/ \binom{N}{m}$$

the average number of particles in equilibrium is always $\theta_0 \equiv 1/2$ and homogeneously distributed regardless of the value of T^z specified by the initial conditions.

3.2. Correlation Functions

Let us introduce briefly some general considerations. The dynamic correlation functions under consideration are defined in the form

$$\langle \mathscr{A}(t)\, \mathscr{B}(0) \rangle \equiv \sum_{m,n} \langle m | \mathscr{A} | m \rangle\, W_{n,m}(t) \langle n | \mathscr{B} | n \rangle\, P_n(0) \tag{26}$$

where $\mathscr{A}$ and $\mathscr{B}$ are diagonal operators in the spin or particle representation $\{|n\rangle\}$ and the sums run over all the possible Ω configurations of a given dynamically invariant subspace. Here $P_n(0)$ is the probability of finding the system in a particular state $|n\rangle$ at $t = 0$ and $W_{n,m}(t)$ denotes the evolution probability from state $|n\rangle$ to state $|m\rangle$ at time t, namely $W_{n,m}(t) = \langle m | e^{-\mathscr{H}t} | n \rangle$.

Conservation of probability requires $\sum_m \langle m | e^{-\mathscr{H}t} | n \rangle \equiv 1 \ \forall\, |n\rangle$; for $\varepsilon = \varepsilon'$ the evolution operator is self-adjoint, consequently the state $|\psi\rangle = \Omega^{-1/2} \sum_n |n\rangle$ satisfies $e^{-\mathscr{H}t} |\psi\rangle = |\psi\rangle$ and therefore is a steady state of the subspace within which the dynamics takes place. Assuming the system is already in *equilibrium* at $t \geqslant 0$, the above probability $P_n(0)$ is simply $1/\Omega$. Since the operators $\mathscr{A}$ and $\mathscr{B}$ are *diagonal*, it is clear that

$\langle\psi|\,\mathscr{A}\,|m\rangle\langle n|\,\mathscr{B}\,|\psi\rangle = \langle m|\,\mathscr{A}\,|m\rangle\langle n|\,\mathscr{B}\,|n\rangle/\Omega$; thus dynamical averages in the steady state become

$$\langle \mathscr{A}(t)\,\mathscr{B}(0)\rangle = \langle\psi|\,\mathscr{A}e^{-\mathscr{H}t}\mathscr{B}\,|\psi\rangle \tag{27}$$

Particle–particle correlation functions $C_{\mathbf{r},\mathbf{r}'}(t) \equiv \langle \hat{\mathscr{N}}_{\mathbf{r}}(t)\,\hat{\mathscr{N}}_{\mathbf{r}'}(0)\rangle - \langle\hat{\mathscr{N}}_{\mathbf{r}}\rangle\langle\hat{\mathscr{N}}_{\mathbf{r}'}\rangle$ in the steady state $|\psi\rangle = |\psi_m\rangle$ constructed above can also be written in terms of dynamical averages such as those of Eq. (27). Here, $\hat{\mathscr{N}}_{\mathbf{r}} = \hat{n}_{\mathbf{r}}$ if $r \in \Lambda_a$ or $\hat{\mathscr{N}}_{\mathbf{r}} = 1 - \hat{n}_{\mathbf{r}}$ if $r \in \Lambda_b$. In what follows, we will assume that both $\mathbf{r}, \mathbf{r}' \in \Lambda_a$, although it is worth pointing out that identical results would arise for all other cases (except for a global change of sign when $\mathbf{r}$ and $\mathbf{r}'$ belong to different sublattices). Inserting a basis of common eigenstates $\{|\mathbf{k}\rangle\}$ of $\mathscr{H}$ and $\mathbf{T}^2$ with eigenvalues $\omega_{\mathbf{k}}$, $T(T+1)$ respectively, it follows that

$$C_{\mathbf{r},\mathbf{r}'}(t) = \sum_{\mathbf{k}\neq\psi_m} \exp(-\omega_{\mathbf{k}}t)\,\langle\psi_m|\,\hat{n}_{\mathbf{r}}\,|\mathbf{k}\rangle\langle\mathbf{k}|\,\hat{n}_{\mathbf{r}'}\,|\psi_m\rangle \tag{28}$$

We have restricted the sum to eigenstates $|\mathbf{k}\rangle$ different from the steady state $|\psi_m\rangle$ (with vanishing eigenvalue) to subtract the time-independent correlations. Selection rules can be applied to simplify this calculation. Noting that the Pauli matrices $\tau_{\mathbf{r}}^z$ are tensors of rank one, since $\hat{n}_{\mathbf{r}} = (1+\tau_{\mathbf{r}}^z)/2$, the Wigner–Eckart theorem ensures nonvanishing matrix elements $\langle\psi_m|\,\hat{n}_{\mathbf{r}}\,|\mathbf{k}\rangle$ only if the total spin T of $|\psi_m\rangle$ and $|\mathbf{k}\rangle$ differs by 0 or 1, i.e., $T = N/2$, $N/2-1$; in either case with $T^z = N/2 - m$.

In order to identify the $|\mathbf{k}\rangle$ states, we first compute the total spin T of a single spin wave $|\varphi_{\mathbf{k}}\rangle = \sum_{\mathbf{r}} \varphi_{\mathbf{k}}(\mathbf{r})\,\tau_{\mathbf{r}}^-\,|\psi_0\rangle$ [where $\varphi_{\mathbf{k}}(\mathbf{r}) = N^{-1/2}\exp(i\mathbf{k}\cdot\mathbf{r})$ for a hypercubic lattice]. Noting that $\mathbf{T}^2 = T^zT^z + \frac{1}{2}(T^+T^- + T^-T^+)$, it follows that

$$\begin{aligned} \mathbf{T}^2\,|\varphi_{\mathbf{k}}\rangle &= \left(\frac{N}{2}-1\right)\frac{N}{2}\,|\varphi_{\mathbf{k}}\rangle, \qquad \mathbf{k}\neq\mathbf{0} \\ \mathbf{T}^2\,|\varphi_0\rangle &= \frac{N}{2}\left(\frac{N}{2}+1\right)|\varphi_0\rangle \end{aligned} \tag{29}$$

The wanted states $|\mathbf{k}\rangle$ giving nonzero matrix elements in Eq. (28) are essentially rotated versions of single-spin-wave states and are the Goldstone bosons of this system. They are generated by applying $(m-1)$ times the lowering operator T^- to the spin waves $|\varphi_{\mathbf{k}}\rangle$,

$$|\mathbf{k}\rangle = A_m(T^-)^{m-1}\,|\varphi_{\mathbf{k}}\rangle \tag{30}$$

where the normalization factor arises from products of the form

$$A_m = \prod_{n=1}^{m-1} \frac{1}{[(N-n-1)n]^{1/2}} = \left[\frac{(N-m-1)!}{(N-2)!\,(m-1)!}\right]^{1/2}, \quad 1 < m < N-1 \tag{31}$$

generated by each application of T^-. However, $|\mathbf{k}=0\rangle = |\psi_m\rangle$ and therefore the states contributing to the sum in Eq. (28) have total spin $T = N/2 - 1$ and total $T^z = N/2 - m$, namely $|\mathbf{k} \neq \mathbf{0}\rangle$. Note that there is an isomorphism between the spin wave states $|\varphi_\mathbf{k}\rangle$ $(\mathbf{k} \neq \mathbf{0})$ and each of the basis vectors spannig the subspace $\{|T, T^z\rangle = |N/2-1, N/2-m\rangle\}$ $(1 < m < N)$. The one-to-one correspondence is obtained by means of the $(T^-)^{m-1}$ and $(T^+)^{m-1}$ operators; therefore the above $|\mathbf{k}\rangle$ states form a *complete* basis for such a subspace.

We are now left with the calculation of $\langle\psi_m|\,\hat{n}_\mathbf{r}\,|\mathbf{k}\rangle$. This matrix element is expanded as

$$\begin{aligned}\langle\psi_m|\,\hat{n}_\mathbf{r}\,|\mathbf{k}\rangle &= A_m \langle\psi_m|\,\hat{n}_\mathbf{r}(T^-)^{m-1}\,|\varphi_\mathbf{k}\rangle \\ &= A_m \sum_\mathbf{p} \varphi_\mathbf{k}(\mathbf{p}) \langle\psi_m|\,\hat{n}_\mathbf{r}(T^-)^{m-1}\,\tau_\mathbf{p}^-\,|\psi_0\rangle \end{aligned} \tag{32}$$

Also,

$$\begin{aligned}\hat{n}_\mathbf{r}(T^-)^{m-1}\,\tau_\mathbf{p}^-\,|\psi_0\rangle &= (m-1)!\,(1-\delta_{\mathbf{r},\mathbf{p}}) \\ &\quad \times \sum_{j_1<j_2<\cdots<j_{m-1}}'' \cdots \sum'' \tau_{\mathbf{r}_{j_1}}^- \cdots \tau_{\mathbf{r}_{j_{m-1}}}^- \tau_\mathbf{p}^-\,|\psi_0\rangle \end{aligned} \tag{33}$$

where the double prime restricts the sums to vectors $\mathbf{r}_j \neq \mathbf{r}, \mathbf{p}$. For $\mathbf{r} \neq \mathbf{p}$ there are $\binom{N-2}{m-1}$ terms contributing equally to $\langle\psi_m|\,\hat{n}_\mathbf{r}\,|\mathbf{k}\rangle$. Hence we obtain

$$\begin{aligned}\langle\psi_m|\,\hat{n}_\mathbf{r}\,|\mathbf{k}\rangle &= (m-1)!\,m! \binom{N-2}{m-1} A_m B_m \sum_\mathbf{p} \varphi_\mathbf{k}(\mathbf{p})(1-\delta_{\mathbf{r},\mathbf{p}}) \\ &= -\left[\frac{m(N-m)}{N(N-1)}\right]^{1/2} \varphi_\mathbf{k}(\mathbf{r}) \end{aligned} \tag{34}$$

where we have used $\sum_\mathbf{r} \varphi_\mathbf{k}(\mathbf{r}) \equiv \sqrt{N}\,\delta_{\mathbf{k},\mathbf{0}}$. Therefore the particle–particle correlations of Eq. (8) are given by

$$C_{\mathbf{r},\mathbf{r}'}(t) = \frac{N}{N-1}\,\tilde{\rho}(1-\tilde{\rho}) \sum_{\mathbf{k}\neq\mathbf{0}} \exp(-\omega_\mathbf{k} t)\,\varphi_\mathbf{k}(\mathbf{r})\,\varphi_\mathbf{k}^*(\mathbf{r}') \tag{35}$$

where $\tilde{\rho} = m/N$ is the density of τ-particles in the sublattice system determined by the initial conditions (not to be confused with the equilibrium coverage θ_0, which is always 1/2).

Since $[\mathscr{H}, T^-] = 0$, the collective states $|\mathbf{k}\rangle$ generated from the single-spin-wave excitations $|\varphi_{\mathbf{k}}\rangle$ [Eq. (30)] share the same *gapless* spectrum $\omega_{\mathbf{k}}$ with low-lying ferromagnetic modes ($\omega_{\mathbf{k}} \sim \mathbf{k}^2$). As was stated above, and as we shall now discuss, these Goldstone excitations give rise to a slow diffusive kinetics with long-time-tail correlations. For a d-dimensional hypercubic lattice with periodic boundary conditions and adsorption–desorption rates ε_j in each of the d principal lattice axes with L_j sites, the eigenenergies are $\omega_{\mathbf{k}} = 2\sum_{j=1}^{d} \varepsilon_j(1-\cos k_j)$, $k_j = 2\pi j/L_j$. In the limit $m \to \infty$, $L_j \to \infty$ with a fixed τ-particle density $\tilde{\rho} = m/N$, finally we obtain

$$C_{\mathbf{r}-\mathbf{r}'}(t) = \tilde{\rho}(1-\tilde{\rho}) \prod_{j=1}^{d} (-1)^{n_j} \exp(-2\varepsilon_j t)\, I_{n_j}(2\varepsilon_j t) \tag{36}$$

where $I_n(z)$ is a modified Bessel function whose integral representations is given by

$$I_n(z) = \frac{1}{\pi}\int_0^{\pi} \exp(z\cos\theta)\cos(\pm n\theta)\, d\theta \tag{37}$$

and $(n_1, n_2, \ldots, n_d) = \mathbf{r} - \mathbf{r}'$ (the lattice constant has been taken as unity). The factors $(-1)^{n_j}$ take into account whether or not $\mathbf{r}$ and $\mathbf{r}'$ belong to different sublattices. In Fig. 1 we show the spreading of the spatial correlations for different times for the case of an isotropic square lattice in the (1, 0) direction [omitting the time-independent prefactor $\tilde{\rho}(1-\tilde{\rho})$].

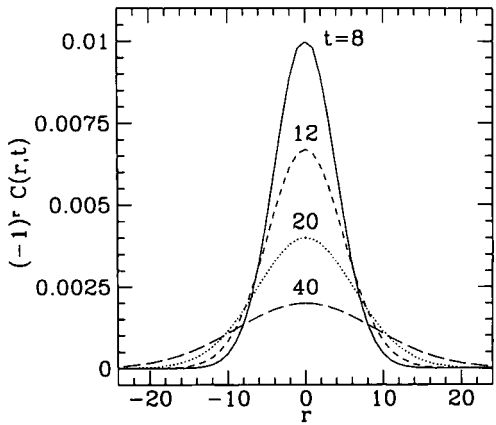

Fig. 1. Particle–particle correlation functions at different times for a square lattice in the (1, 0) direction.

The long-time behavior ($\varepsilon_j t \gg 1 \; \forall \varepsilon_j$) of autocorrelation functions ($\mathbf{r} = \mathbf{r}'$) can be obtained from the corresponding asymptotic expansion of $I_0(z)$.[21] This results in long-time diffusive tails with a power law asymptotic kinetics given by

$$C(t) \simeq A t^{-d/2} + \mathcal{O}(t^{-(d+2)/2})$$
$$A = \frac{\tilde{\rho}(1-\tilde{\rho})}{2^d \pi^{d/2}} \prod_{j=1}^{d} \frac{1}{\sqrt{\varepsilon_j}} \tag{38}$$

An interesting feature arises when the deposition–evaporation rates are highly anisotropic. In that case the autocorrelation function may display different regimes undergoing crossovers through effective spatial dimensionalities. For instance, if $\varepsilon_j/\varepsilon_{j+1} \gg 1$, recalling that

$$I_0(z) \simeq 1 + \frac{z^2}{4} + \mathcal{O}(z^4), \qquad z \ll 1$$
$$I_0(z) \simeq \frac{\exp(z)}{(2\pi z)^{1/2}} \left[1 + \frac{z^{-1}}{8} + \mathcal{O}(z^{-2}) \right], \qquad z \gg 1 \tag{39}$$

we can readily identify $d-1$ crossover times $t_1^* \ll t_2^* \ll \cdots \ll t_{d-1}^*$ defined by $t_j^* = (4\pi\varepsilon_{j+1})^{-1}$ such that $C(t) \simeq A_j t^{-j/2}$ within the range $t_{j-1} \ll t \ll t_j$

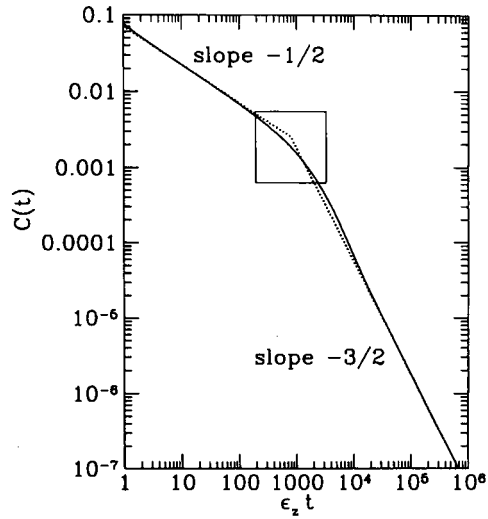

Fig. 2. Crossover of autocorrelation function for $\varepsilon_x = \varepsilon_y = 10^{-4}$, $\varepsilon_z = 1$. The square indicates the region $[t^* = (4\pi\varepsilon_x)^{-1}]$ where the asymptotic behavior (denoted by the dotted lines) changes from one- to three-dimensional form.

and effective amplitudes $A_j = \tilde{\rho}(1-\tilde{\rho})(4\pi)^{-j/2} \prod_{k=1}^{j} \varepsilon_k^{-1/2}$. This feature is shown in Fig. 2, where we display the crossover of $C(t)$ which undergoes a kinetic transition from one to three spatial dimensions in a dimer system with $\varepsilon_x = \varepsilon_y \ll \varepsilon_z$. Direct numerical tests of this behavior are very difficult to implement, given the long-time scales involved.

4. FINITE-SIZE SCALING AND MONTE CARLO SIMULATIONS FOR DIMERS AND TRIMERS

The diffusive behavior discussed so far has been rigorously established for a dimer system with equal deposition–evaporation rates. In this section we provide numerical evidence supporting the validity of the diffusive picture in more general situations by means of finite-size scaling arguments. Based on the exact results of Section 3 it is worthwhile to see first how finite-size scaling properties emerge in the case $\varepsilon = \varepsilon'$. On general grounds, we expect that these ideas may be applied for $\varepsilon \neq \varepsilon'$ as well, eventually using different scaling functions.

From Eq. (35) it is clear that the autocorrelation function of a finite system with $N = L_1 L_2 \cdots L_d$ sites can be expressed as

$$C(t) = \frac{\tilde{\rho}(1-\tilde{\rho})}{N-1} \left\{ \prod_{j=1}^{d} \sum_{n=0}^{L_j-1} \exp\left[-2\varepsilon_j \left(1 - \cos\frac{2\pi n}{L_j} \right) t \right] - 1 \right\} \tag{40}$$

where the last term cancels the contribution of $|\mathbf{k} = \mathbf{0}\rangle = |\psi_m\rangle$. In the scaling limit, $L_j \to \infty$, $\varepsilon_j t \to \infty$ $\forall j$ (i.e., $t \gg t^*_{d-1}$) with $y_j \equiv t/L_j^z$ held constant, it can be easily checked that the autocorrelation function satisfies the finite-size scaling form

$$C(L_1, \ldots, L_d, t) = t^{-\gamma_d} Y(y_1, \ldots, y_d) \tag{41}$$

where the universal scaling function Y is given by

$$\begin{aligned} Y(y_1, \ldots, y_d) &= \tilde{\rho}(1-\tilde{\rho}) \prod_{i=1}^{d} (y_i)^{1/2} \left(\prod_{j=1}^{d} \vartheta_3(q_j) - 1 \right) \\ q_j &\equiv \exp(-4\pi^2 \varepsilon_j y_j) \end{aligned} \tag{42}$$

and $\vartheta_3(q)$ is the Jacobi theta function of the third kind[21]

$$\vartheta_3(q) \equiv 1 + 2 \sum_{n=1}^{\infty} q^{n^2} \tag{43}$$

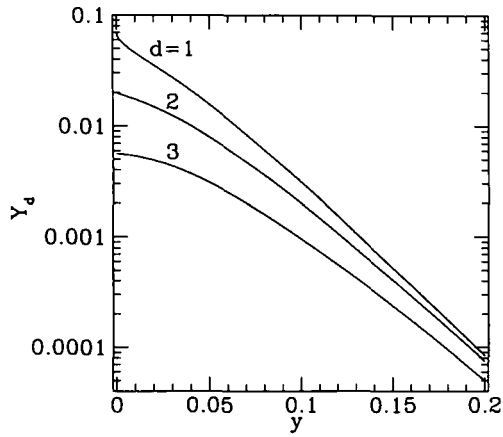

Fig. 3. Particle–particle scaling functions for one-, two-, and three-dimensional isotropic lattices. The asymptotic slope yields the diffusion constant associated with nonequilibrium density fluctuations.

Then, it is clear that the critical exponents of the dimer model turn out to be $\gamma_d = d/2$, $z = 2$. Notice that

$$\lim_{y_j \to 0^+} (y_j)^{1/2} \vartheta_3(q_j) = \frac{1}{2(\pi\varepsilon_j)^{1/2}} \tag{44}$$

and therefore $Y(0^+,\ldots,0^+)$ yields the asymptotic autocorrelation amplitude already found in the infinite system [Eq. (38)]. The particle–particle scaling function also embodies information regarding the nonequilibrium dynamics. For instance, the diffusion constants associated with the density fluctuations can be read off from the asymptotic behavior of $Y(\mathbf{y})$, namely

$$D_j = -\frac{1}{4\pi^2} \lim_{\{y_l\} \to \infty} \frac{\partial}{\partial y_j} \ln Y(\mathbf{y}) \tag{45}$$

To extract any D_j, the limit here has to be taken by specifying appropriate ratios of the L_l in such a way that $\varepsilon_j y_j$ is the minimum of all the $\{\varepsilon_j y_j\}$. In Fig. 3 we show these scaling functions for isotropic lattices ($y_j = y = t/L^2$) in $d = 1, 2, 3$.

4.1. Dimers

In view of the slow kinetic character of this model, Monte Carlo simulations in two- and higher-dimensional lattices of relatively large sizes

are not feasible to implement without using considerable amounts of computing time. Even in one dimension,[16] numerical studies of sufficiently high quality turn out to be very time-consuming. However, the finite-size scaling of autocorrelation functions motivates a numerical simulation of the general case $\varepsilon \neq \varepsilon'$ using *smaller* systems, thus overcoming in part the above difficulties.

The simulation procedure in a square lattice goes as follows. In the initial stage of the algorithm we consider an empty surface of size $L \times L$ with $L = 10$, 14, 20 and periodic boundary conditions; thus the value of T^z is chosen to be zero ($\tilde{\rho} = 1/2$). Isotropic deposition and evaporation attempts are randomly made choosing from the $2L^2$ bonds of the lattice. If the selected bond is empty, a deposition is attempted with probability ε. Similarly, an evaporation attempt with probability ε' takes place provided the chosen bond is already occupied with *two* particles. If neither deposition nor evaporation is possible, the bond state is unchanged. These mutually exclusive attempts, either successful or not, are repeated $2L^2$ times, after which the time is increased in one unit (of course, intermediate measurements on time intervals not smaller than $L^{-2}/2$ can be also attained). The system is conducted through this process during a time t_0 larger than the corresponding relaxation time until a stationary regime is

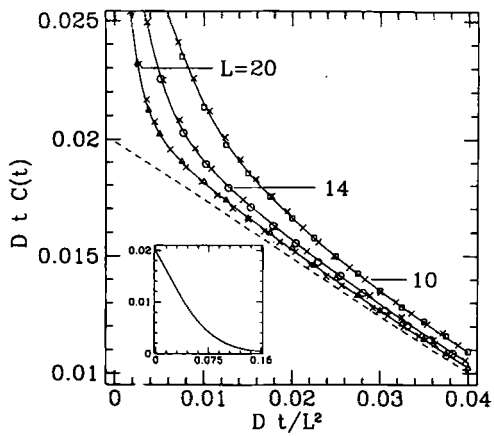

Fig. 4. Evidence of finite-size scaling and universality of autocorrelation functions for dimers on a square lattice in the steady state. The data were averaged over 10^7 histories starting from an initially empty lattice with $L \times L$ sites, $L = 10$, 14, and 20. The solid lines are the theoretical values [Eq. (40)]. Open symbols denote the results for $\varepsilon'/\varepsilon = 1$, whereas the crosses indicate the results for $\varepsilon'/\varepsilon = 1/2$. The data collapse toward a universal scaling curve indicated by the dashed line [Eq. (42)], which is displayed in a wider range in the inset at the bottom left.

obtained. The measuring of autocorrelation functions is then carried out by averaging on different samples or histories.

Since the characteristic sizes we used are small, the self-averaging is rather poor and therefore a relatively large number of samples is needed to obtain reliable measurements. In all cases, we used 10^7 histories, which turns out to be sufficient to yield excellent agreement with the theoretical results given by Eqs. (40) and (41). This is shown in Fig. 4. Furthermore, not only is the case $\varepsilon = \varepsilon'$ consistent with the above expectations, but also the case of different deposition–evaporation rates. Our data suggest that the *same* scaling function [Eq. (42)] can be used to fit the numerical results by sliding the curves sideways and upward on each scale using the actual diffusion constant $D = D(\varepsilon, \varepsilon')$ as a metric factor, i.e., $D^{d/2}C(L, t) = t^{-d/2}Y(Dt/L^2)$. Thus, our results not only provide evidence of finite-size scaling, but also of universality on ε and ε' in the isotropic case. On the other hand, these phenomenological considerations turn out to be in very good agreement with the diffusion constants resulting from alternative approaches to be introduced in Section 5.

We have also considered the case of adsorption–desorption of dimers on a triangular lattice. In this case the continuous rotation symmetry around the z axis referred to in Section 2.2 is absent, as the lattice geometry is not bipartite. The asymptotic kinetics in this situation seems difficult to solve by analytical means, as we cannot easily identify constants of motion. However, in view of the removal of the above symmetry, we might expect a fast asymptotic behavior. To eludicate this question we have conducted

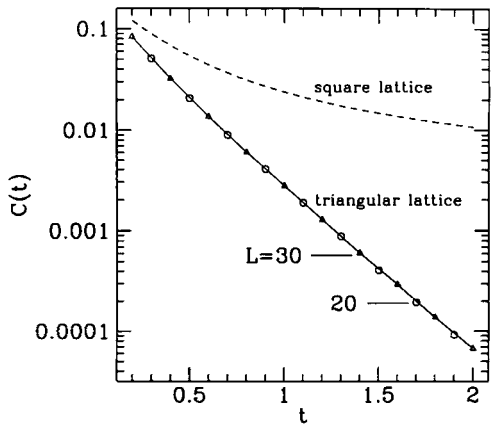

Fig. 5. Exponentially fast decay of autocorrelation functions for dimers in a triangular lattice (open symbols). The averages were taken on 10^7 samples with $L \times L$ sites, $L = 20, 30$. The dashed line indicates the theoretical slow diffusive decay resulting in a square lattice.

Monte Carlo simulations in this system using the same microscopic rules described above but with $3L^2$ deposition–evaporation attempts per unit time on each of the $3L^2$ bonds of the triangular lattice. The results, shown in Fig. 5, strongly suggest an exponentially fast kinetics. The data are rather insensitive to the lattice size, consistent with a size-independent gap width in the spectrum of the associated evolution operators.

4.2. Trimers

The trimer system is much harder to deal with analytically, partly due to the fact that there are many more disconnected subspaces. This rather complex situation is typical for k-mers for $k \geqslant 3$. Even in one dimension the full phase space splits into a very large number of dynamically invariant subspaces.[16] In contrast to the dimer case, this number grows exponentially with the size of the system[17] and therefore numerical studies will be strongly affected by the choice of initial conditions. The question regarding the complete classification of *all* invariant subspaces by universality classes needs further clarification from analytical approaches, as the problem is numerically intractable. Nevertheless, there is some evidence from previous studies in one-dimensional models suggesting that the trimer system may exhibit a nondiffusive behavior for particular initial configurations. On the other hand, as long as the Goldstone symmetry referred to in Section 2.2 is not violated by the interplay between the lattice structure and the k-mer shape, a slow asymptotic dynamics with power law decaying correlations might be expected in general.

Bearing these considerations in mind, for the sake of practicality we will restrict considerations to triangular trimers depositing and evaporating from an initially empty two-dimensional triangular lattice with periodic boundary conditions and $\varepsilon = \varepsilon'$. This choice corresponds to the largest subspace where analytical approaches are more difficult. To avoid mismatch of the three associated sublattices (and therefore the removal of the Goldstone symmetry), the number of sites in the horizontal lattice direction should be an integer multiple of three, whereas along the vertical direction the number of sites should be even to allow for appropriate periodic boundary conditions. To implement the already introduced finite-size scaling techniques using a *single* length scale, we have used lattices of $L \times L$ sites with $L = 6\times$ integer. We carried out Monte Carlo simulations for sizes $L = 6$, 12, 18, 30, sampling over 10^7 histories to overcome the poor self-averaging properties of the rather small sizes. The simulation procedure is analogous to that described in Section 4.1 except that the time is increased by one step after $2L^2$ random attempts to deposit or evaporate triangular plaquettes on the $2L^2$ triangular faces of the lattice.

Assuming the finite-size scaling hypothesis also holds in this case, we expect that in the steady state the particle–particle autocorrelation function $C(L, t)$ will satisfy $C(L, t) \sim t^{-\gamma} F(t/L^z)$ for $t \to \infty$, $L \to \infty$, and t/L^z held constant. The data collapse toward a single universal scaling function F shown in Fig. 6a indicates strongly that this is the case. This collapse is attained on choosing the set of dynamical critical exponents $\gamma = 1$, $z = 2$; thus autocorrelations are dominated by a Goldstone slow dynamics which

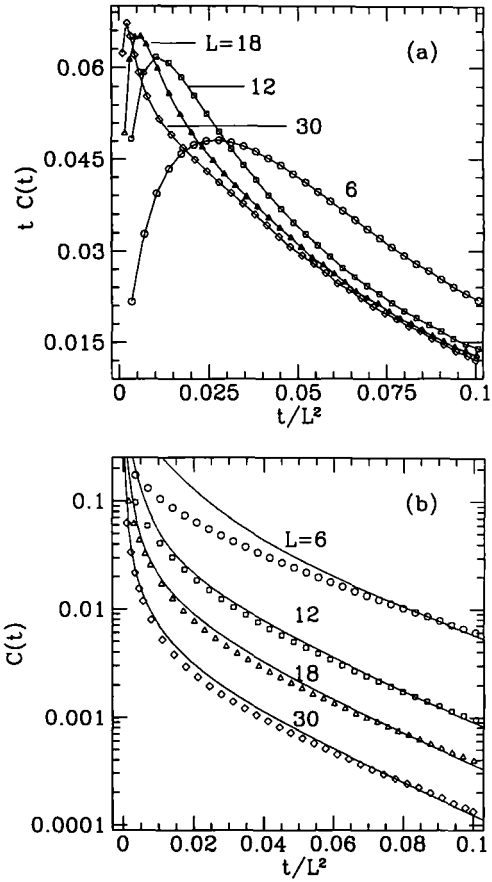

Fig. 6. (a) Evidence of finite-size scaling and diffusive behavior for autocorrelation functions obtained by deposition and evaporation of triangular trimers on the triangular lattice in the steady state. The data have been averaged over 10^7 histories starting from an empty lattice of $L \times L$ sites for $L = 6$, 12, 18, 30. The data collapse is obtained on choosing a dynamical critical exponent $z = 2$. (b) Exponential regime of autocorrelation functions. The open symbols denote the numerical results, whereas the solid lines are the analytical values obtained in the dimer system [Eq. (40)] after renormalizing both scales. The asymptotic slopes are $4\pi^2 D \log_{10} e$.

turns out to be of diffusive type once again. Moreover, Fig. 6b provides further evidence of universality as the *same* scaling functions, obtained analytically for dimers in the square lattice, can be used (after rescaling both axes with nonuniversal metric factors) to fit the numerical data of the triangular lattice within the regime $t \sim L^2$, where the finite-size scaling hypothesis is valid. The metric factor along the time scale is the diffusion constant ($D \simeq 3\varepsilon$) corresponding to the subspace explored. Unlike the dimer system with equal deposition–evaporation rates, the diffusion constant of the trimer model is strongly dependent on the choice of the initial conditions or subspace where the evolution takes place. A contrasting example yielding a different diffusion constant for a nearly jammed isotropic background configuration will be discussed in Section 5.3.

The diffusive picture discussed so far probably still holds in the limit $\varepsilon' \to 0^+$, but the case $\varepsilon' \equiv 0$ is entirely different. This situation is the prototype "deposition-only" model introduced by Flory and Renyi and generalized later for studying random sequential adsorption on surfaces. Starting from an empty triangular lattice, a very large number of jammed states can be obtained, none of which contains a vacant triangular plaquette. Figure 7 displays one such jammed configuration.

A simple-minded mean-field approach would give a mean saturation coverage $\theta_0 = 1$, whereas the result from the average of 500 samples with 900×900 sites yields $\theta_0 \sim 0.79(7)$. Indeed, this is an indication of strong fluctuation effects. Note that a nonzero but small value of ε' is associated with a crossover time $t^* \sim 1/\varepsilon'$. For $t \ll t^*$ the probability of evaporation at a given site is very small, thus Flory-like states are approached within the regime $1/\varepsilon \ll t \ll t^*$. However, over much longer time scales $t \gg t^*$ the steady

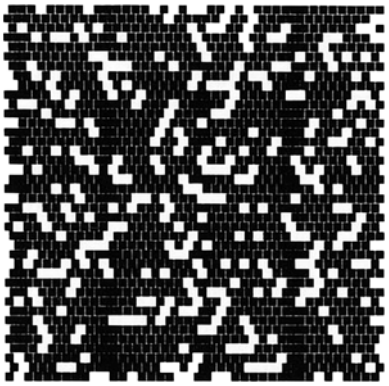

Fig. 7. Particular fully jammed configuration of triangular trimers in the triangular lattice. The mean coverage resulting from the average of 500 samples with 900×900 sites is 0.79(7).

state changes dramatically to yield a saturation coverage close to unity. The diffusive behavior is only valid within that asymptotic regime. On the other hand, the configuration space of the system will break up into a larger number of disconnected subspaces when either of the rates ε or ε' is zero.

5. MEAN-FIELD, SPIN WAVE, AND RANDOM WALK APPROACHES

In this section we use the mean-field method, spin wave theory, and the random walk approach to treat diffusive properties of the system in more general cases with anisotropic and unequal deposition–evaporation rates. Some comparisons will be made with the results in the previous sections. The spin wave and random walk approaches are exact, but are limited to nearly jammed simple backgrounds. The mean-field approach does not have this limitation, and will be seen to recover the exact results for dimers in situations where the other two methods allow a check. It also provides the steady-state coverage. Most of the results obtained in this section can be readily generalized to higher dimensions. For simplicity, we will mainly discuss two-dimensional cases.

5.1. Mean-Field Method for Dimers on Square and Honeycomb Lattices

Consider the square lattice shown in Fig. 8a. In the sublattice mapped particle representation, deposition of a dimer is then equivalent to a hopping process from the mapped site to the unmapped site, and evaporation to a hopping in the opposite direction. Therefore the particle conservation gives the following equation for the particle density $\tilde{\rho}_{n,m}(t)$ at an unmapped site ($n+m=$ an even integer):

$$\frac{\partial \tilde{\rho}_{n,m}}{\partial t} = \varepsilon_x(1-\tilde{\rho}_{n,m})(\tilde{\rho}_{n-1,m}+\tilde{\rho}_{n+1,m}) + \varepsilon_y(1-\tilde{\rho}_{n,m})(\tilde{\rho}_{n,m-1}+\tilde{\rho}_{n,m+1})$$

$$-\varepsilon'_x\tilde{\rho}_{n,m}(2-\tilde{\rho}_{n-1,m}-\tilde{\rho}_{n+1,m}) - \varepsilon'_y\tilde{\rho}_{n,m}(2-\tilde{\rho}_{n,m-1}-\tilde{\rho}_{n,m+1}) \quad (46)$$

A similar equation is obtained for a mapped site ($n+m=$ an odd integer) by the simple exchange ($\varepsilon \leftrightarrow \varepsilon'$) in the above equation. These equations lead to exponential decay of the particle density, as discussed also in a recent publication by Krapivsky and Ben-Naim,[22] where the dynamics of the coverage before the saturation is calculated for a continuous model.

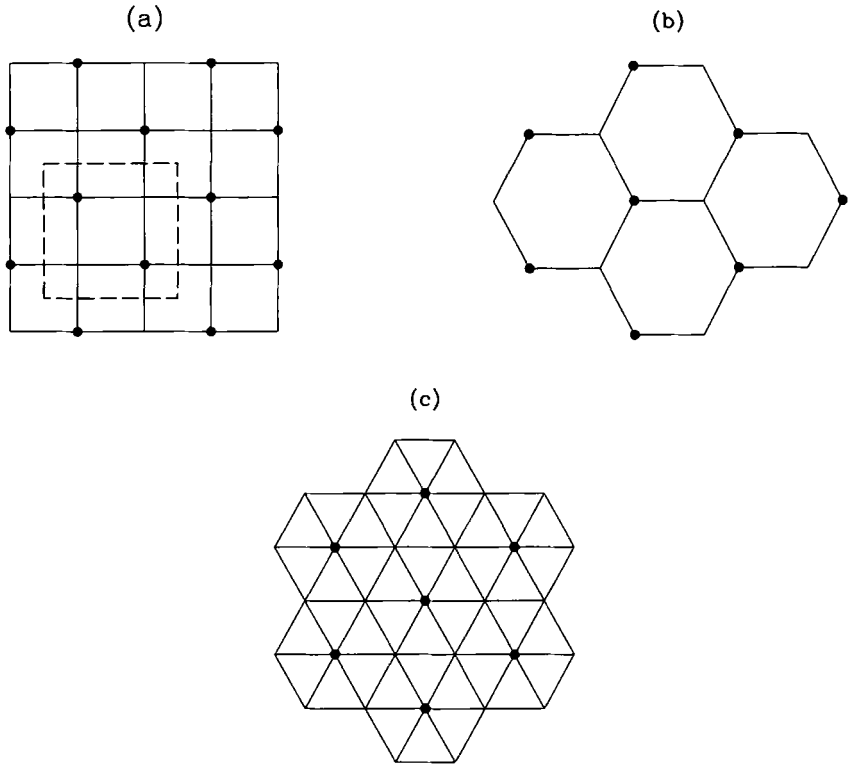

Fig. 8. Schematic view of isotropic fully jammed configurations for (a) dimers on the square lattice (the dashed line denotes the unit cell used in the text), (b) dimers on a honeycomb lattice, and (c) triangular trimers on a triangular lattice.

In a steady state, these two equations each reduce to an identical statement relating the uniform densities in the mapped (M) and the unmapped (U) sublattices:

$$\tilde{\rho}_M \varepsilon_x - \tilde{\rho}_U \varepsilon'_x - \tilde{\rho}_U \tilde{\rho}_M (\varepsilon_x - \varepsilon'_x) + \tilde{\rho}_M \varepsilon_y - \tilde{\rho}_U \varepsilon'_y - \tilde{\rho}_U \tilde{\rho}_M (\varepsilon_y - \varepsilon'_y) = 0 \quad (47)$$

Due to the fact that different initial configurations may belong to different and disconnected subspaces (see discussions in Section 2), the steady-state coverage depends on the initial condition from which the system started to evolve. For simplicity as well as practicality, we now consider the case when the system starts with an empty lattice, which leads to $\tilde{\rho}_U = 1 - \tilde{\rho}_M$ in the sublattice mapped representation. From the

steady-state equation (47), we find that the coverage for the isotropic case is given by

$$\theta = \frac{1}{2}\left[\tilde{\rho}_{\mathrm{U}} + (1 - \tilde{\rho}_{\mathrm{M}})\right] = \frac{1}{1 + (\varepsilon'/\varepsilon)^{1/2}} \tag{48}$$

which agrees with the Monte Carlo simulations, and is consistent with the analytic result for the case of equal deposition–evaporation rates given earlier. However, notice that when $\varepsilon' \equiv 0$ the mean-field scheme fails to give the correct mean coverage. This is the Flory situation discussed in Section 4.2. Starting from an empty two-dimensional square lattice, the actual mean coverage in the isotropic case with $\varepsilon' = 0$ has a saturation value of 0.906(8), which evidently is not obtained from Eq. (48). In the following considerations we will assume nonzero deposition–evaporation rates.

To calculate the diffusion constants, we consider small fluctuations about the steady-state densities. Assuming both the temporal and spatial dependences are small, we write the particle density for an unmapped site as

$$\tilde{\rho}_{n,m}(t) = \tilde{\rho}_{\mathrm{U}} + \sum_{q_x, q_y, E} A_{\mathrm{U}}(q_x, q_y, E)\, e^{2i(q_x n + q_y m)} e^{-Et} \tag{49}$$

and a similar one for a mapped site with small fluctuation $A_{\mathrm{M}}(q_x, q_y, E)$ about the steady-state density $\tilde{\rho}_{\mathrm{M}}$. Substituting them into Eq. (46) and eliminating the ratio $A_{\mathrm{M}}/A_{\mathrm{U}}$, one obtains the dispersion relation

$$\begin{aligned}(E - \alpha_x - \alpha_y)(E - \beta_x - \beta_y) = {} & [\alpha_x \cos(2q_x) + \alpha_y \cos(2q_y)] \\ & \times [\beta_x \cos(2q_x) + \beta_y \cos(2q_y)]\end{aligned} \tag{50}$$

with

$$\begin{aligned}\alpha_x &= 2[\varepsilon_x - \tilde{\rho}_{\mathrm{U}}(\varepsilon_x - \varepsilon_x')], \qquad \alpha_y = 2[\varepsilon_y - \tilde{\rho}_{\mathrm{U}}(\varepsilon_y - \varepsilon_y')] \\ \beta_x &= 2[\varepsilon_x' + \tilde{\rho}_{\mathrm{M}}(\varepsilon_x - \varepsilon_x')], \qquad \beta_y = 2[\varepsilon_y' + \tilde{\rho}_{\mathrm{M}}(\varepsilon_y - \varepsilon_y')]\end{aligned} \tag{51}$$

In the long-wavelength limit (small q_x and q_y), the low-lying mode becomes

$$E \simeq D_x q_x^2 + D_y q_y^2 \tag{52}$$

with the diffusion constants in the two directions given by

$$D_x = \frac{2(2\alpha_x\beta_x + \alpha_x\beta_y + \alpha_y\beta_x)}{\alpha_x + \alpha_y + \beta_x + \beta_y}, \qquad D_y = \frac{2(2\alpha_y\beta_y + \alpha_y\beta_x + \alpha_x\beta_y)}{\alpha_x + \alpha_y + \beta_x + \beta_y} \tag{53}$$

Some special cases can now be discussed. First, we consider the case of equal deposition–evaporation rates, but allowing them to be different in different directions in space ($\varepsilon = \varepsilon'$). The dispersion becomes, using Eq. (51),

$$E \simeq 4\varepsilon_x q_x^2 + 4\varepsilon_y q_y^2 \tag{54}$$

This is the case discussed in Section 4.1 by means of finite-size scaling arguments [Eq. (45)]. The results agree with each other.

The next situation is when the deposition rate is different from the evaporation rate, but the system is isotropic in space ($\varepsilon_x = \varepsilon_y = \varepsilon$; $\varepsilon'_x = \varepsilon'_y = \varepsilon'$). If the steady state is reached from the initial empty lattice (in the original particle representation), we can use Eqs. (51) and (48) to obtain

$$E \simeq 4(\varepsilon'\varepsilon)^{1/2}(q_x^2 + q_y^2) \tag{55}$$

This result is also in very good agreement with the Monte Carlo simulations combined with the finite-size scaling and universality considerations discussed in Section 4.

The mean-field method can be applied to dimers on other bipartite lattices, e.g., the honeycomb lattice. A similar derivation leads to the following equation for the dispersion relation:

$$\left\{E - \sum_{i=1}^{3} [(1-\tilde{\rho}_U)\varepsilon_i + \varepsilon'_i \tilde{\rho}_U]\right\}\left\{E - \sum_{i=1}^{3} [(1-\tilde{\rho}_M)\varepsilon'_i + \varepsilon_i \tilde{\rho}_M]\right\}$$
$$= \sum_{i=1}^{3}\sum_{j=1}^{3} [(1-\tilde{\rho}_U)\varepsilon_i + \varepsilon'_i \tilde{\rho}_U][(1-\tilde{\rho}_M)\varepsilon'_j + \varepsilon_j \tilde{\rho}_M]$$
$$\times \exp[i\mathbf{q}\cdot(\boldsymbol{\delta}_i - \boldsymbol{\delta}_j)] \tag{56}$$

where $\tilde{\rho}_U$ and $\tilde{\rho}_M$ are the steady-state particle densities for the two sublattices in the sublattice mapped representation. The three vectors $\{\boldsymbol{\delta}_i\}$ denote the nearest-neighbor bonds in three orientations in the honeycomb lattice, with corresponding anisotropic deposition–evaporation rates $(\varepsilon_i, \varepsilon'_i)$ along each type of bond, respectively.

This result can be compared with the exact calculation in Section 5.3 for the special background of $\tilde{\rho}_M \simeq \tilde{\rho}_U \simeq 1$ (or 0)—there is complete agreement, showing that the mean-field method is exact for this case. Note also that E determined in the above equation is in general complex (although always with a positive real part), and the consequence of this will be discussed in more detail in Section 5.3 together with dimers on general bipartite lattices in nearly jammed cases.

5.2. Spin Wave Analysis for Dimers on the Square Lattice

We next explore the spin wave analogy of the system. Again, we consider the general situations when both the spatial anisotropy and the unequal deposition–evaporation rates are allowed. For the case of dimers on square lattice, the "Hamiltonian" [Eq. (22) in Section 2.1] can be written as

$$\begin{aligned} H = \tfrac{1}{4} \sum_{n,m} & [(\varepsilon_x + \varepsilon'_x)(1 - \boldsymbol{\tau}_{n,m} \cdot \boldsymbol{\tau}_{n+1,m}) + (\varepsilon_y + \varepsilon'_y)(1 - \boldsymbol{\tau}_{n,m} \cdot \boldsymbol{\tau}_{n,m+1}) \\ & - 2(-1)^{n+m} (\varepsilon_x - \varepsilon'_x)(\tau^z_{n,m} + \tau^+_{n,m} \tau^-_{n+1,m} - \tau^-_{n,m} \tau^+_{n+1,m}) \\ & - 2(-1)^{n+m} (\varepsilon_y - \varepsilon'_y)(\tau^z_{n,m} + \tau^+_{n,m} \tau^-_{n,m+1} - \tau^-_{n,m} \tau^+_{n,m+1})] \end{aligned} \tag{57}$$

Here the sublattice-mapped "spin" variables $\boldsymbol{\tau}_{n,m}$ are related to the $\sigma_{n,m}$ through the transformation described at the beginning of the previous section; see Eq. (21). A spin wave description (or equivalently "random walk" approach like that in Section 5.3) can then be applied to the "nearly" jammed states. For example, we can use $|0\rangle$ to denote the fully jammed state with all spins up in terms of τ-spin variables (or $\tilde{\rho}_{n,m} = 1$, for any n, m in the sublattice mapped particle representation). Then the single-spin-flip state $|n, m\rangle = \tau^-_{n,m} |0\rangle$ will evolve according to the following relation:

$$\begin{aligned} H |n, m\rangle = & \varepsilon_x (2 |n, m\rangle - |n+1, m\rangle - |n-1, m\rangle) \\ & + \varepsilon_y (2 |n, m\rangle - |n, m+1\rangle - |n, m-1\rangle) \end{aligned} \tag{58}$$

for $n + m =$ an even integer. The equation for $n + m =$ an odd integer can be similarly obtained and the result is equivalent to replacing ε_x, ε_y by ε'_x, ε'_y in the above equation. For simplicity, we choose the unit cell to consist of four sites as shown in Fig. 8a, and write

$$|n, m\rangle_i = A_i \exp[i2(q_x n + q_y m)] \tag{59}$$

where i runs from 1 to 4 in the unit cell. Substituting it into the eigenvalue equation $H |n, m\rangle = E |n, m\rangle$ and using Eq. (57), we determine the secular dispersion relation by

$$\begin{aligned} & \{[E - 2\varepsilon_x - 2\varepsilon_y][E - 2\varepsilon'_x - 2\varepsilon'_y] \\ & \quad - [2\varepsilon_x \cos(2q_x) - 2\varepsilon_y \cos(2q_y)][2\varepsilon'_x \cos(2q_x) - 2\varepsilon'_y \cos(2q_y)]\} \\ & \quad \times \{[E - 2\varepsilon_x - 2\varepsilon_y][E - 2\varepsilon'_x - 2\varepsilon_y] - [2\varepsilon_x \cos(2q_x) + 2\varepsilon_y \cos(2q_y)] \\ & \quad \times [2\varepsilon'_x \cos(2q_x) + 2\varepsilon'_y \cos(2q_y)]\} = 0 \end{aligned} \tag{60}$$

The first factor gives no acoustic branch, while from the second one we can obtain for small q_x and q_y

$$E \to D_x q_x^2 + D_y q_y^2 \tag{61}$$

where the diffusion constants are

$$D_x = 4\frac{2\varepsilon_x\varepsilon_x' + \varepsilon_x\varepsilon_y' + \varepsilon_x'\varepsilon_y}{\varepsilon_x + \varepsilon_y + \varepsilon_x' + \varepsilon_y'}, \qquad D_y = 4\frac{2\varepsilon_y\varepsilon_x' + \varepsilon_x\varepsilon_y' + \varepsilon_x'\varepsilon_y}{\varepsilon_x + \varepsilon_y + \varepsilon_x' + \varepsilon_y'} \tag{62}$$

This result is again consistent with what we obtained using the mean-field method in Eq. (53). For dimers on the simple cubic lattice in three dimensions we can similarly use n, m, and l to label the x, y, and z axes, respectively. The two sublattices are then distinguished by $n+m+l=$ an even or an odd integer. The spin wave method can be applied to dimers on any bipartite lattice and to other cases treated in the next subsection by the analogous but slightly simpler random walk method.

5.3. The Random Walk Approach on Nearly Jammed Configurations

For states near jammed configurations of a simple, e.g., periodic type, simulations show that the time evolution involves the diffusion of active patches which are locally unjammed. An example of such an active patch is the single spin flip on the fully jammed parallel spin state discussed in the previous subsection. The spin wave treatment given there is equivalent to a random walk, as is the diffusive behavior of small fluctuations about the steady-state densities in the mean-field approach.

In this subsection a direct random walk approach is used to treat exactly the diffusive behavior for nearly jammed configurations of sufficiently simple sort and to provide insights for more complicated situations.

5.3.1. Dimers on Nearly Jammed Bipartite Lattices. We now consider the jammed state in a *bipartite* two-dimensional lattice, with sublattices A and B fully occupied and unoccupied, respectively (see, for example, Figs. 8a and 8b). We treat here the nearby state unjammed by removing one particle from sublattice A, at site $\mathbf{i}$, say. We denote this state by $\mathbf{i}$, and the probability of its occupancy at time t by $P(\mathbf{i}, t)$. No dimers are present to evaporate in this state. The vectors δ_j^A $(j=1,\ldots, z)$ from site $\mathbf{i}$ to its z nearest-neighbor sites $\mathbf{j}$ (on sublattice B) label the z bonds joining pairs of vacant nearest-neighbor sites available for deposition of a dimer. Such deposition takes place with anisotropic (but translationally invariant) rates $\varepsilon(\delta_j^A)$, say. Suppose deposition occurs on the bond joining $\mathbf{i}$ to the

particular nearest neighbor **j**. That gives a state, hereafter denoted by **j**, which differs from the "full A, empty B" jammed state by an extra particle at site **j** (on sublattice B). Denote by $Q(\mathbf{j}, t)$ the probability of this state at time t.

For any site **j** on sublattice B, there is a set of z vectors δ_l^B to its nearest neighbors on sublattice A. State **j** can evolve only by evaporation of a dimer, i.e., by emptying the occupied pair of sites joined by one of the vectors δ_l^B [rate $\varepsilon(\delta_l^B)$]. That gives a state $\boldsymbol{l}$ ($\boldsymbol{l}$ on sublattice A). However, the state $\boldsymbol{l}$ could have arisen at time t from dimer evaporation from any occupied bond joining $\boldsymbol{l}$ to its nearest neighbors, so its probability $P(\boldsymbol{l}, t)$ is given by the master equation

$$P(\boldsymbol{l}, t) = P(\boldsymbol{l}, t-1)\left[1 - \frac{1}{z}\sum_{n=1}^{z} \varepsilon(\boldsymbol{\delta}_n^N)\right] + \frac{1}{z}\sum_{n=1}^{z} \varepsilon(\boldsymbol{\delta}_n^B)\, Q(\boldsymbol{l} - \boldsymbol{\delta}_n^B, t-1) \tag{63}$$

(where the time step has been taken as unity). Similarly **j** arises from deposition onto any vacant bond incident on **j**, so $Q(\mathbf{j}, t)$ satisfies the master equation

$$Q(\mathbf{j}, t) = P(\mathbf{j}, t-1)\left[1 - \frac{1}{z}\sum_{n=1}^{z} \varepsilon(\boldsymbol{\delta}_n^A)\right] + \frac{1}{z}\sum_{n=1}^{z} \varepsilon(\boldsymbol{\delta}_n^A)\, P(\mathbf{j} - \boldsymbol{\delta}_n^A, t-1) \tag{64}$$

These equations are linear difference equations with constant coefficients, since the rates are translationally invariant. So they can be solved by the substitution

$$\begin{aligned} P(\boldsymbol{l}, t) &= e^{-Et} e^{i\mathbf{q}\cdot\boldsymbol{l}} P_{\mathbf{q}} \\ Q(\mathbf{j}, t) &= e^{-Et} e^{i\mathbf{q}\cdot\mathbf{j}} Q_{\mathbf{q}} \end{aligned} \tag{65}$$

(for any $\boldsymbol{l}$, **j** on sublattices A and B, respectively), **q** is any vector consistent with (periodic) boundary conditions, and E will be a function of **q**.

The equations arising from inserting (65) into the master equations are

$$\begin{aligned} [e^{-E} - 1 + \varepsilon'(0)]\, P_{\mathbf{q}} &= \varepsilon'(\mathbf{q})\, Q_{\mathbf{q}} \\ [e^{-E} - 1 + \varepsilon(0)]\, Q_{\mathbf{q}} &= \varepsilon(\mathbf{q})\, P_{\mathbf{q}} \end{aligned} \tag{66}$$

where $\varepsilon(\mathbf{q})$, $\varepsilon'(\mathbf{q})$ are defined by

$$\varepsilon(\mathbf{q}) = \frac{1}{z}\sum_{n=1}^{z} \varepsilon(\boldsymbol{\delta}_n^A)\exp(-i\mathbf{q}\cdot\boldsymbol{\delta}_n^A)$$
$$\varepsilon'(\mathbf{q}) = \frac{1}{z}\sum_{n=1}^{z} \varepsilon(\boldsymbol{\delta}_n^B)\exp(-i\mathbf{q}\cdot\boldsymbol{\delta}_n^B) \tag{67}$$

The resulting secular equation for E is

$$[e^{-E} - 1 + \varepsilon'(0)][e^{-E} - 1 + \varepsilon(0)] = \varepsilon(\mathbf{q})\,\varepsilon'(\mathbf{q}) \tag{68}$$

The spectrum of excitation energies $E = E(\mathbf{q})$ consists of two branches, the lower of which is gapless because of the broken symmetry. The long-time behavior comes from the low-energy modes, which arises from the lower branch at small $\mathbf{q}$, where

$$E(\mathbf{q}) \sim \frac{\varepsilon(0)\,\varepsilon'(0) - \varepsilon(\mathbf{q})\,\varepsilon'(\mathbf{q})}{\varepsilon(0) + \varepsilon'(0)} \sim i\alpha\cdot\mathbf{q} + \mathbf{q}\cdot\Delta\cdot\mathbf{q} + \cdots \tag{69}$$

Here α is nonzero for the general anisotropic and unequal-rate cases on lattices without inversion symmetry. α clearly provides an oscillatory time dependence for the solutions of the form (65), while Δ provides the damping. They relate, respectively, to the ballistic velocity and diffusion constant of *biased* diffusion. This process can be seen very simply in the random walk arising in the picture given above for the special case of the honeycomb lattice. When deposition is allowed on bonds of only one orientation and evaporation from bonds only of the other two orientations, a walk arises which is diffusive in one of the three lattice directions and purely ballistic in an orthogonal direction. If one of the two evaporation rates is set to zero, the diffusive element of the walk disappears and the process becomes purely deterministic.

For the case of isotropic rates, $\varepsilon(\mathbf{q}) = \varepsilon\gamma(\mathbf{q})$, $\varepsilon'(\mathbf{q}) = \varepsilon'\gamma'(\mathbf{q})$, where

$$\gamma(\mathbf{q}) = \frac{1}{z}\sum_{n=1}^{z}\exp(i\mathbf{q}\cdot\boldsymbol{\delta}_n^A), \qquad \gamma'(\mathbf{q}) = \frac{1}{z}\sum_{n=1}^{z}\exp(i\mathbf{q}\cdot\boldsymbol{\delta}_n^B) \tag{70}$$

and the ballistic component disappears.

For the square lattice

$$\gamma(\mathbf{q}) = \gamma'(\mathbf{q}) = \tfrac{1}{2}(\cos q_x + \cos q_y) \to 1 - \tfrac{1}{4}q^2, \qquad q \to 0 \tag{71}$$

so for isotropic rates the diffusion constants of the square lattice are

$$D_x = D_y = \frac{\varepsilon\varepsilon'}{2(\varepsilon+\varepsilon')} \tag{72}$$

The anisotropic result (61) of Section 5.2 can easily be obtained from the general result (69) above.

For the honeycomb lattice with isotropic rates,

$$\gamma(\mathbf{q}) = [\gamma'(\mathbf{q})]^*, \qquad 1 - |\gamma(\mathbf{q})|^2 \to \tfrac{1}{2}q^2, \qquad q \to 0 \tag{73}$$

so D_x and D_y are also given by Eq. (72). The anisotropic generalizations can again be readily obtained from (69).

The description just given applies for dimers on bipartite lattices in any dimension. It verifies for these cases that the mean-field approach given in Section 5.1 provides exact diffusion constants.

5.2.2. Triangular Trimers on the Triangular Lattice. The second type of application of the random walk approach is to plaquette k-mers on a simple nearly jammed background.

To be specific we consider the case of the triangular lattice (Fig. 8c) with trimers corresponding to particles at the vertices of one elementary triangular face of the lattice. The jammed state shown in Fig. 8c can be unjammed by removing one particle, at site $\mathbf{n}$ say. The resulting state is denoted by $\mathbf{n}$, and the probability of its occurrence at time t by $P(\mathbf{n}, t)$.

A trimer can be deposited on any of the six triangles with a vertex at $\mathbf{n}$. It is convenient to distinguish these triangles by the six vectors $\boldsymbol{\delta}_j$, $j = 1, 2, \ldots, 6$, joining $\mathbf{n}$ to the closest occupied sites in Fig. 8c. Consider the new state obtained by deposition on the triangle specified by a particular $\boldsymbol{\delta}_j$. We label this state, for reasons of symmetry, by $\mathbf{n} + \frac{1}{2}\boldsymbol{\delta}_j$ and denote its probability by $Q_j(\mathbf{n} + \frac{1}{2}\boldsymbol{\delta}_j, t)$. It can evolve by either evaporating the trimer first deposited or the one containing the particle at vertex $\mathbf{n} + \boldsymbol{\delta}_j$. So a pair of master equations can be obtained relating the probabilities P and Q.

For isotropic deposition and evaporation rates $\varepsilon, \varepsilon'$, the master equation takes the form

$$\begin{aligned} P(\mathbf{n}, t) &= P(\mathbf{n}, t-1)(1-\varepsilon') + \frac{\varepsilon'}{6}\sum_{j=1}^{6} Q_j\left(\mathbf{n} + \frac{1}{2}\boldsymbol{\delta}_j, t-1\right) \\ Q_j(\mathbf{m}, t) &= Q_j(\mathbf{m}, t-1)(1-\varepsilon) \\ &\quad + \frac{\varepsilon}{2}\left[P\left(\mathbf{m} - \frac{1}{2}\boldsymbol{\delta}_j, t-1\right) + P\left(\mathbf{m} + \frac{1}{2}\boldsymbol{\delta}_j, t-1\right)\right] \end{aligned} \tag{74}$$

These equations can be reduced by the substitution

$$P(\mathbf{n}, t) = e^{-Et} e^{i\mathbf{q}\cdot\mathbf{n}} P_{\mathbf{q}}$$
$$Q_j(\mathbf{m}, t) = e^{-Bt} e^{i\mathbf{q}\cdot\mathbf{m}} Q_{j,\mathbf{q}} \tag{75}$$

It then becomes evident that the j dependence of $Q_{j,\mathbf{q}}$ is contained in a factor $\cos(\frac{1}{2}\mathbf{q}\cdot\boldsymbol{\delta}_j)$, so the resulting form of the master equation is

$$[e^{-E} - 1 + \varepsilon'] P_{\mathbf{q}} = \varepsilon' \gamma(\mathbf{q}) Q_{\mathbf{q}}$$
$$[e^{-E} - 1 + \varepsilon] Q_{\mathbf{q}} = \varepsilon P_{\mathbf{q}} \tag{76}$$

where

$$Q_{j,\mathbf{q}} = Q_{\mathbf{q}} \cos(\tfrac{1}{2}\mathbf{q}\cdot\boldsymbol{\delta}_j), \qquad \gamma_{\mathbf{q}} = \tfrac{1}{6} \sum_{j=1}^{6} \cos^2(\tfrac{1}{2}\mathbf{q}\cdot\boldsymbol{\delta}_j) \tag{77}$$

The long-time behavior is again determined by the low-energy spectrum, which comes from the small-q limit of a gapless "Goldstone" branch

$$E(q) \sim \frac{\varepsilon\varepsilon'[1-\gamma(\mathbf{q})]}{\varepsilon+\varepsilon'} \sim Dq^2 \tag{78}$$

The diffusion constant is

$$D = \frac{\delta^2 \varepsilon\varepsilon'}{8(\varepsilon+\varepsilon')} \tag{79}$$

where δ is the length of the vectors $\boldsymbol{\delta}_j$.

This type of discussion readily generalizes to the anisotropic case, and to some other plaquette k-mers on other lattices. An example with similarities to the case first discussed is a symmetric triangular trimer deposited and evaporated on a simple nearly jammed state of a face-centered square lattice. The initial state is obtained by filling all except one of the face-centered sites with a particle of type α. The trimer is based on an isosceles triangle with hypotenuse equal to the lattice constant. An α-particle is at the right angle vertex and β-particles occupy the other two vertices. The detailed analysis is exactly analogous to that in the case discussed above, and similar equations apply, but with the replacement of the six vectors $\boldsymbol{\delta}_j$ by four vectors joining a face center to its nearest-neighbor face centers.

Another tractable example with interesting properties involves the cross-shaped 5-mer formed by particles at one site and its four nearest neighbors on a square lattice. This is deposited and evaporated on the nearly jammed state of the square lattice obtained initially by removing one particle from an otherwise completely filled A sublattice, with sublattice B empty. It is straightforward to show that the diffusion process is composed of two one-dimensional random walks along the two axes through **n**. In the case of a generalized starting unjammed state with a low concentration of vacancies on the A sublattice (and sublattice B empty), the diffusion occurs along a random rectangular network with nodes at the A sublattice vacancies.

The random walk approach suggests that the diffusive behavior is very general in the long-time limit, where the concentration of active patches is low and their interaction insignificant. However, there exist exceptions, like the ballistic case discussed above and an example (trimers in a one-dimensional system with a ferro–antiferro domain wall) whose finite-size behavior does not collapse using the t/L^2 variable associated with pure diffusion.

6. CONCLUSIONS

This study has confirmed that two- and higher-dimensional deposition–evaporation systems share many of the principal characteristics seen in the one-dimensional cases. These include strong nonergodicity for $k \geqslant 3$, manifested by the breakup of the phase space into exponentially many invariant subspaces, and related to the existence of exponentially many jammed states in the Flory limit.

Also shared is the possibility of slow long-time dynamics, which arises from a Goldstone symmetry and appears to be diffusive for empty lattice initial conditions. This is in agreement with recent work of Dhar and Barma,[17] and shows in one dimension that a larger class of initial conditions gives subdiffusive behavior (the autocorrelation function decays as $t^{1/4}$). This and other new behaviors are also not ruled out in higher dimensions: For triangular trimers on a triangular lattice, for example, one could expect logarithmic corrections.

In two dimensions, special relationships of k-mer shape and lattice type have to exist for the Goldstone symmetry and the consequent slow dynamics. So, dimer systems only have the Goldstone symmetry on higher-dimensional lattices which are bipartite (as the linear chain is). More generally, a lattice which can be divided into k sublattices has the Goldstone symmetry for k-mers whose shape is such that, wherever placed on the lattice, the k-mer covers one site of each sublattice. Examples are

linear or triangular trimers in the triangular lattice. The numerical studies give clear evidence for the Goldstone slow dynamics, and the exact random walk arguments confirm this for simple backgrounds. On the contrary, the expected fast (exponential) decay is seen in numerical results for a systems without this symmetry, namely dimers on the triangular lattice.

An important result for the one-dimensional case which has here been generalized to higher dimensions is the exact form for the autocorrelation functions for dimers deposited and evaporated with equal rates on bipartite lattices. In this case the Goldstone symmetry is part of a full rotation symmetry, and, as in the one-dimensional case, it is this which is exploited in the analysis. The result is of diffusive character. For the hypercubic lattices the autocorrelation function is a product of one-dimensional forms. This can contain crossovers not present in one dimension. Anisotropy in rates is a source of such crossovers. It has been shown that when the anisotropy is sufficiently strong it divides the evolution into a sequence of power law decays each associated with the lattice dimension then effective in the diffusion.

Lattice anisotropy also reveals other new phenomena not previously seen in the deposition–evaporation systems. One is biased diffusion. This was discovered in mean-field and exact random walk treatment for lattices without inversion symmetry, for unequal anisotropic rates. The evolution can become a deterministic ballistic process in extreme examples such as the honeycomb lattice with deposition and evaporation of dimers at unique unequal bond orientations. Though not observed previously in the investigation of one-dimensional system, the biased diffusion can occur there, e.g., for chains with alternating rates.

The techniques used in this study merit some further discussion here. The most comprehensive exact treatment, concerning the autocorrelation functions, applies in the most restricted model, dimers with anisotropic but equal rates (on bipartite lattices). Spin wave and random walk approaches are still exact, and not limited to equal rates, and the latter can apply to a wider variety of systems (k-mers, for example). However, some other conditions, particularly the need for nearly jammed backgrounds, are more restrictive. The mean-field approach is limited to the dimer case, but allows any rates and background. It gives exact results for the long-time diffusive decays in simple cases where an exact check exists.

The numerical techniques are widely applicable to more general situations where analytical methods are difficult to implement. This is the case of unjammed subspaces, where the concepts of random walker and spin waves are not always well defined. These techniques assume it is possible to trace a path of active patches in an otherwise jammed background. However, for $k \geqslant 3$ it can be readily shown that a "single" walker may

eventually split into many other walkers. In principle there is no reason to assume that even in a finite and well-defined walker density regime, interactions and collisions among walkers do not change the asymptotic kinetic behavior. In this sense, our numerical simulations combined with finite-size scaling techniques have supported the diffusive picture in such complex situations. They have also confirmed the crucial role of the Goldstone symmetry in the slow asymptotic dynamics. A complete classification of all subspaces by universality classes is unlikely to be obtained by numerical means, as for $k \geqslant 3$ the number of dynamically invariant subspaces grows exponentially with the size of the system.[17] Each subspace involves a massive computation on its own, so it has not been possible to extend further our work as in the one-dimensional case.

Despite the considerable number of exact and accurate results provided by these techniques, the richness and diversity of the systems leaves a number of unanswered questions. While the Goldstone arguments imply power law asymptotic decay in a large class of systems, it is not clear that the asymptotic behavior is always diffusive, for $k > 2$ or even for $k = 2$, $\varepsilon \neq \varepsilon'$ with anisotropic rates. Nevertheless, for the isotropic case and $k = 2$ our simulations provided evidence of universal diffusive behavior. In the one-dimensional work, the finite-size scaling studies gave strong evidence that except in one case (trimers in a special initial state) the systems were all in one universality class, characterized by length-scaling exponent $z = 2$, and so strongly suggestive of diffusion. The evidence for this in the two-dimensional study is less strong, despite the very extensive numerical work. And the study has shown that there are some special (Goldstone) evaporation–deposition systems which are purely ballistic, i.e., in a separate universality class from diffusion.

Another unanswered question concerns spatial correlations. Pilot investigations, for example in dimer systems, have indicated that the spatial correlations in the steady state are often of uninteresting δ-function type. Whether this is universally the case is not known and deserves attention.

Further generalization of the models is desirable, to make them of wider applicability and more realistic for such processes as catalysis. Mixing k-mers with k'-mers is clearly desirable in this context, and whether k and k' share a common factor is important for the Goldstone symmetry.

Previous work has considered deposition models with nearest-neighbor exclusion. A detailed extension of our work to this case is desirable. Already one can see that some conclusions will generalize. In particular, if the Goldstone symmetry (and consequent slow dynamics) is present in the system without nearest-neighbor exclusion, it also occurs in the system with it. The reason is that in the quantum spin Hamiltonian the nearest-neighbor exclusion introduces only further "projection" factors which are products of

operators all of the form $(1 \pm \sigma_{\mathbf{r}}^{z})$. These factors are invariant under the spin rotation associated with the Goldstone symmetry, and therefore preserve it. Further details are under investigation. The one-dimensional case with single defect bond has already been studied analytically.[23] The exact solution to the autocorrelation function exhibits time regimes characterized by different exponential decay rates. Other generalizations are to introduce energetic considerations and to include disorder and nonequilibrium aspects and the effects of driving the systems. The effect of disorder on dimer systems in bipartite lattices is presently being considered, and an account of the driven steady state in one-dimensional deposition and evaporation systems will be published elsewhere.

ACKNOWLEDGMENTS

It is a pleasure to acknowledge fruitful discussions with M. Barma, C. D. Fosco, and D. Ko. We also thank J. W. Evans for sending us a copy of his review before publication. N.N.C. and M.D.G. are grateful to the Scientific and Engineering Research Council for financial support under grant GR/G02727.

REFERENCES

1. N. G. van Kampen, *Stochastic Processes in Physics and Chemistry*, 2nd ed. (North-Holland, Amsterdam, 1992).
2. T. Hwa and M. Kardar, *Phys. Rev. Lett.* **62**:1813 (1989).
3. M. Kardar, G. Parisi, and Y. C. Zhang, *Phys. Rev. Lett.* **56**:889 (1986).
4. B. Derrida, M. R. Evans, V. Hakim, and V. Pasquier, *J. Phys. A: Math. Gen.* **26**:1493 (1993).
5. J. M. Carlson, J. T. Chayes, E. R. Grannan, and G. H. Swindle, *Phys. Rev. Lett.* **65**:2547 (1990).
6. P. Bak, C. Tang, and K. Wiesenfeld, *Phys. Rev. Lett.* **59**:381 (1987).
7. M. C. Bartelt and V. Privman, *Int. J. Mod. Phys. B* **5**:2883 (1991).
8. J. W. Evans, *Rev. Mod. Phys.* **65**:1281 (1993).
9. P. J. Flory, *J. Am. Chem. Soc.* **61**:1518 (1939).
10. A. Renyi, *Publ. Math. Inst. Hung. Acad. Sci.* **3**:109 (1958); *Selected Transl. Math. Stat. Prob.* **4**:205 (1963).
11. R. M. Ziff, E. Gulari, and Y. Barshad, *Phys. Rev. Lett.* **56**:2553 (1988).
12. D. Ben-Avraham and J. Kohler, *J. Stat. Phys.* **65**:839 (1991).
13. R. Dickman and R. Burschka, *Phys. Lett. A* **127**:132 (1988).
14. A. H. Bretag, B. R. Davis, and D. I. B. Kerr, *J. Membr. Biol.* **16**:363 (1974).
15. A. H. Bretag, C. A. Hurst, and D. I. B. Kerr, *J. Chem. Biol.* **73**:367 (1978).
16. M. Barma, M. D. Grynberg, and R. B. Stinchcombe, *Phys. Rev. Lett.* **70**:1033 (1993); R. B. Stinchcombe, M. D. Grynberg, and M. Barma, *Phys. Rev. E* **47**:4018 (1993).
17. D. Dhar and M. Barma, *Pramana-J. Phys.* **41**:L193 (1993); TIFR preprint TH/94-02.
18. E. R. Cohen and H. Reiss, *J. Chem. Phys.* **38**:680 (1963).
19. J. Goldstone, A. Salam, and S. Weinberg, *Phys. Rev.* **127**:965 (1962).

20. S. Abers and B. W. Lee, *Phys. Rep.* **9**:1 (1973); N. N. Bogoliubov, *Lectures in Statistical Physics*, Vol. 2 (Gordon and Breach, London, 1970); also see P. W. Anderson, *Concepts in Solids—Lectures on the Theory of Solids* (Benjamin, New York, 1963).
21. M. Abramowitz and I. A. Stegun, eds., *Handbook of Mathematical Functions* (Dover, New York, 1958).
22. P. L. Krapivsky and E. Ben-Naim, *J. Chem. Phys.* **100**(9):6778 (1994).
23. Niu-Niu Chen and R. B. Stinchcombe, *Phys. Rev. E* **49**:2784 (1994).